Aqueous Photocurrent Measurements Correlated to Ultrafast Electron Transfer Dynamics at Ruthenium Tris Diimine Sensitized NiO Photocathodes

Nicolas Queyriaux, Ruri A. Wahyuono, Jennifer Fize, Corinne Gablin, Maria Wächtler, Eugenie Martinez, Didier Léonard, Benjamin Dietzek, Vincent Artero, Murielle Chavarot-Kerlidou

Published in final edited form as:
J Phys Chem C Nanomater Interfaces. 2017 March 23; 121(11): 5891–5904. doi:10.1021/acs.jpcc.6b12536.

Aqueous Photocurrent Measurements Correlated to Ultrafast Electron Transfer Dynamics at Ruthenium Tris Diimine-Sensitized NiO Photocathodes

Nicolas Queyriaux[#a], **Ruri A. Wahyuono**[#b,c], **Jennifer Fize**[a], **Corinne Gablin**[d], **Maria Wächtler**[b,c], **Eugénie Martinez**[e], **Didier Léonard**[d,*], **Benjamin Dietzek**[b,c,*], **Vincent Artero**[a], and **Murielle Chavarot-Kerlidou**[a,*]

[a]Laboratoire de Chimie et Biologie des Métaux, UMR 5249 University Grenoble Alpes, CNRS, CEA, 17 rue des Martyrs, 38000 Grenoble, France

[b]Leibniz Institute of Photonic Technology (IPHT) Jena e. V., Albert-Einstein-Strasse 9, Jena 07745, Germany

[c]Institute for Physical Chemistry and Center for Energy and Environmental Chemistry, Friedrich Schiller University Jena, Helmholtzweg 4, Jena 07743, Germany

[d]Institut des Sciences Analytiques, UMR 5280 (Université Claude Bernard Lyon 1 /CNRS / ENS de Lyon), 5 rue de la Doua, 69100 Villeurbanne, France

[e]CEA, Leti, MINATEC Campus, 17 rue des Martyrs, 38054 Grenoble Cedex 9, France

[#] These authors contributed equally to this work.

Abstract

Understanding the structural and electronic factors governing the efficiency of dye-sensitized NiO photocathodes is essential to optimize solar fuel production in photoelectrochemical cells (PECs). For these purpose, three different ruthenium dyes, bearing either two or four methylphosphonate anchoring groups and either a bipyridine or a dipyridophenazine ancillary ligand, were synthesized and grafted onto NiO films. These photoelectrodes were fully characterized by XPS, ToF-SIMS, UV-vis absorption, time-resolved emission and femtosecond transient absorption spectroscopies. Increasing the number of anchoring groups from two to four proved beneficial for the grafting efficiency. No significant modification of the electronic properties compared to the parent photosensitizer was observed, in accordance with the non-conjugated nature of the grafted linker. The photoelectrochemical activity of the dye-sensitized NiO electrodes was assessed in fully aqueous medium in the presence of an irreversible electron acceptor and photocurrents reaching 190 μA.cm^{-2} were recorded. The transient absorption study revealed the presence of two charge recombination pathways for each of the sensitizers and evidenced a stabilized charge separated state in the dppz derivative, supporting its superior photoelectrochemical activity.

[*]**Corresponding Authors**: Didier Leonard; didier.leonard@univ-lyon1.fr; Benjamin Dietzek; benjamin.dietzek@leibniz-ipht.de; Murielle Chavarot-Kerlidou; murielle.chavarot-kerlidou@cea.fr.

Notes

The authors declare no competing financial interest.

Europe PMC Funders Author Manuscripts

Introduction

In the context of global energy demand, the construction of tandem dye-sensitized photoelectrochemical cells (DS-PECs) for solar hydrogen production or carbon dioxide reduction is promising, yet challenging.1–6 Their design is based on the assembly of two photoelectrodes, a photoanode driving the oxidation of water into oxygen in order to supply the photocathode with protons and electrons to achieve proton and/or CO_2 reduction. In this approach, an efficient grafting of molecular photosensitizers and/or (photo)catalysts onto a suitable metal oxide electrode is mandatory. The strategy behind the success of the dye-sensitized solar cells,7,8 pioneered by Grätzel, based on the covalent grafting of carboxylate-9 or phosphonate-substituted10 dyes onto a suitable semiconducting metal oxide, was applied first to the construction of various dye-sensitized photoanodes.11–26 On the other hand, dye-sensitized photocathodes for H_2 production6,27–33 or CO_2 reduction34,35 emerged more recently. They all rely on nickel oxide (NiO), which is a low-cost and easy-to-process *p*-type semiconductor, suitable for hole injection into its valence band.5 Various nanostructured NiO film preparations have been reported over the years and recently evaluated with respect to their performance as photocathodes in a comprehensive benchmarking study.36 Ruthenium tris-diimine complexes were often employed as sensitizers for NiO29,30,32,35 and combined to suitable catalysts according to three different architectures of dye-sensitized H_2-evolving photocathodes: grafting of a covalent photocatalyst,29,35 co-grafting of photosensitizer and catalyst30 or layer-by-layer assembly of the latter.32

One important drawback limiting the efficiency of NiO-based photocathodes is the fast recombination occurring, after the initial hole injection, between the hole in the semiconductor and the reduced photosensitizer.37 Structural optimizations of the latter were thus reported in order to slow down this process, detrimental for photoelectrochemical activity. As far as ruthenium photosensitizers are concerned,38–46 the group of F. Odobel first established that the insertion of a non-conjugated spacer, methylene group typically, between the anchoring function and the complex could favourably decrease the electronic coupling with NiO.38,39 In a related approach, Wu and coworkers increased the length of the conjugated spacer between the semiconductor surface and a cyclometalated ruthenium photosensitizer.40 Elegant molecular engineering, based on the dyad concept, was also independently developed by the groups of L. Hammarström and Y. Wu, to delocalize the charge on the reduced dye away from the surface.41–43 While complex architectures with optimized push-pull character have been proposed, Bräutigam and colleagues alternatively showed that asymmetric substitution of the paradigmatic $Ru(bpy)_3$-core is already sufficient to induce an asymmetric metal-to-ligand charge transfer in the photosensitizer, which in turn influences the hole injection process characteristics.44 These Ru-sensitized photocathodes, nevertheless, exhibit a large discrepancy in their recombination kinetics, ranging from a few hundred of ps40,43,44 to μs.41 This suggests that some recombination pathways can be overlooked, as recently highlighted for an organic dye-sensitized NiO electrode.47 These results also reflect the fact that charge recombination is an intricate process, still matter of debate as for its underlying mechanisms;48 a deeper understanding of the various

parameters controlling interfacial electron transfer at dye-sensitized NiO electrodes is thus required in order to optimize their efficiency for solar fuel production.

Herein, we report the preparation and characterization of nanostructured NiO films sensitized by a series of phosphonate-substituted ruthenium polypyridyl complexes. Special attention was paid to the number of phosphonate anchoring groups carried by the photosensitizer (four *versus* two) and to the nature of the third diimine ligand. The π-accepting dipyridophenazine (dppz) ligand was selected as a model system, prefiguring charge transfer properties which could favorably remove the electron density of the reduced dye away from the NiO surface. The resulting photoelectrodes were characterized by various techniques, including surface mass spectrometry analysis (ToF-SIMS). Their photoelectrochemical activity was assessed under aqueous conditions and the dynamics of the corresponding interfacial electron transfers was investigated by time-resolved emission and ultrafast transient absorption spectroscopy.

Experimental section

Synthesis and dye-sensitized NiO film preparation

All reagents were purchased from Sigma-Aldrich and used as obtained unless otherwise stated. Reagent-grade solvents were used without further purification. The 4,4′-bis(diethylphosphonomethyl)-2,2′-bipyridine ligand (4,4′-$(CH_2PO_3Et_2)_2$-bpy) was custom-synthesized by the company Azasynth, according to a previously reported procedure.49 The dipyrido[3,2-a:2’,3’-c]phenazine (**dppz**) ligand,50 $[Ru(bpy)_3](PF_6)_2$,51 $[Ru(bpy)_2(dppz)](PF_6)_2$50 and $[Ru(4,4′-(CH_2PO_3H_2)_2\text{-bpy})(bpy)_2](PF_6)_2$ (**RuP_2^{OEt}-bpy**)49 were synthesized according to reported procedures. NiO films (two layers, screen-printed onto conductive glass) were purchased from Dyenamo AB, Stockholm, Sweden. ^1H and ^{13}C NMR spectra were recorded at 298 K on a Bruker Avance 300 MHz spectrometer. NMR data are referenced to the residual solvent peak and reported in relative to tetramethylsilane reference (δ = 0 ppm). UV-vis absorption spectra were recorded either on a Shimadzu UV-1800 spectrometer (complexes in solution) or on an Agilent Cary 60 UV-Vis spectrometer equipped with a solid sample holder. ESI-MS measurements were carried out on a Thermoquest Finnigan LCQ spectrometer.

General Procedure for the synthesis of [Ru(4,4′-$(CH_2PO_3Et_2)_2$-bpy)$_2$(N^N)]$(PF_6)_2$ (N^N: **bpy** or **dppz**): A solution of commercially available $Ru(dmso)_4Cl_2$ (420 mg, 0.88 mmol) and 4,4′-$(CH_2PO_3Et_2)_2$-bpy (800 mg, 1.75 mmol) in methanol (100 mL) was refluxed overnight under argon. Removal of the solvent and drying under vacuum yielded the dark-red highly hygroscopic intermediate $[Ru(4,4′-(CH_2PO_3Et_2)_2\text{-bpy})_2Cl_x(DMSO)_{2-x}]Cl_{2-x}$. This intermediate was not purified and could be stored in the dark under argon for weeks. A solution of $[Ru(4,4′-(CH_2PO_3Et_2)_2\text{-bpy})_2Cl_x(DMSO)_{2-x}]Cl_{2-x}$ (1 equivalent, using an average molecular weight) and N^N (1 equivalent) in a water/ethanol (1:3) mixture was refluxed overnight. After cooling down to room temperature, 5 mL of a saturated KPF_6 aqueous solution was added to the reaction mixture. Extraction with dichloromethane and removal of the organic solvent yield a crude reddish solid. After purification by flash chromatography on silica gel (MeCN/aqueous KNO_3 (0.4 M), 80:20) followed by anion

metathesis, [Ru(4,4′-$(CH_2PO_3Et_2)_2$-bpy)$_2$(N^N)]$(PF_6)_2$ (**RuP_4^{OEt}-bpy** and **RuP_4^{OEt}-dppz**) were isolated as red powders.

RuP_4^{OEt}-bpy (60%) ^{1}H-NMR (300 MHz, CD_3CN): δ (ppm) 8.46 (d, *J* = 8.1 Hz, 2H), 8.37 (s, 4H), 8.01 (t, *J* = 7.8 Hz, 2H), 7.66 (d, *J* = 5.0 Hz, 2H), 7.60 (d, *J* = 5.4 Hz, 4H), 7.43 – 7.33 (m, 2H), 7.30 (s, 4H), 4.15 – 3.80 (m, 16H), 3.35 (d, J_{PH} = 22.5 Hz, 8H), 1.32 – 0.95 (m, 24H).^{13}C-NMR (75 MHz, CD_3CN): δ (ppm) C_q: 158.0, 157.5, 151.5, 151.4, 151.2, 146.1, 146.0, 145.96, 145.9, 137.8, 128.7, 128.6, 127.5, 126.2, 125.3, 124.3, 62.5, 62.4, 33.5, 31.7, 16.6, 15.7. *ESI-MS: m/z* 585.3 $[M–2PF_6]^{2+}$. HRMS (ESI): calcd for $C_{50}H_{68}N_6O_{12}P_4Ru$ ($[M–2PF_6]^{2+}$): *m/z* 585.143910; found: 585.144699.

RuP_4^{OEt}-dppz (55 %) *^{1}H-NMR (300 MHz,CD_3CN)*: δ (ppm) 9.67 (d, *J* = 8.2 Hz, 2H), 8.47 (s, 4H), 8.43 (s, 2H), 8.20 – 8.10 (m, 4H), 7.90 (dd, *J* = 8.2, 5.4 Hz, 2H), 7.76 (d, *J* = 5.8 Hz, 2H), 7.63 (d, *J* = 5.9 Hz, 2H), 7.42 (d, *J* = 5.8 Hz, 2H), 7.20 (d, *J* = 5.8 Hz, 2H), 4.00 (d, *J* = 29.8 Hz, 16H), 3.39 (dd, *J* = 27.1, 22.6 Hz, 8H), 1.26 – 1.01 (m, 24H). *^{13}C-NMR (75 MHz,CD_3CN)*: δ (ppm) 157.8, 157.5, 154.6, 152.8, 152.4, 151.5, 146.2, 143.8, 141.0, 134.4, 133.5, 132.0, 130.7, 129.6, 128.4, 126.2, 63.5, 34.5, 32.7, 16.7. ESI-MS: *m/z* 648.1 $[M–2PF_6]^{2+}$. HRMS (ESI): calcd for $C_{58}H_{70}N_8O_{12}P_4Ru$ ($[M–2PF_6]^{2+}$): *m/z* 648.154809; found: 648.155499.

Hydrolysis of the phosphoester groups in **RuP_2^{OEt}-bpy**, **RuP_4^{OEt}-bpy** and **RuP_4^{OEt}-dppz** was performed as previously reported for [Ru(4,4′-$(CH_2PO_3H_2)_2$-bpy)$(bpy)_2$]Cl_2.49

Preparation and sensitization of pristine NiO films—The screen-printed two layers NiO plates were annealed at 450°C for 30 minutes applying the following temperature protocol: from room temperature to 450°C in 30 minutes, 450°C for 30 minutes, gentle return to room temperature.36 The resulting NiO electrodes were soaked into methanolic solutions (10^{-4} M) of **RuP_2^{OEt}-bpy**, **RuP_4^{OEt}-bpy** or **RuP_4^{OEt}-dppz** for 24 hours on an orbital stirring table. The electrodes were then sequentially rinsed with methanol and acetone to remove the physisorbed dyes, before being dried in a stream of argon.

Electrochemical measurements

Electrochemical analysis was performed using a BioLogic SP300 potentiostat controlled via the EC-Lab® V10 software. Cyclic voltammetry experiments were recorded in a classical single-compartment three-electrode cell combining a glassy carbon or a platinum working electrode, a platinum wire counter-electrode and a custom-made Ag/AgCl reference electrode (separated from the solution by a Vycor frit). Typical measurements were carried out at room temperature using 3 mL of argon-purged acetonitrile solution (0.1 M *n*-Bu_4NBF_4 as supporting electrolyte) of 1 mM of the complex. Measurements were corrected for ohmic drop. Ferrocene was finally added at the end of each measurement as an internal reference, allowing every measured value to be referenced versus the Fc^+/Fc redox couple. Photocurrent measurements were carried out in a custom-made single-compartment cell,52 using a typical three-electrode configuration combining the dye-sensitized NiO film as working electrode, a platinum wire counter-electrode and a custom-made Ag/AgCl reference electrode (separated from the solution by a Vycor frit). Before each experiment, the Ag/AgCl reference electrode was externally calibrated using $K_3[Fe(CN)_6]$ in potassium

phosphate buffer (0.1 M, pH = 7). The surface of the working electrode in contact with the electrolyte was 0.50 cm^2. Sodium acetate buffer (0.1 M, pH = 4.5; prepared by acidification with HCl of a 0.1 M sodium acetate aqueous solution) and potassium phosphate buffer (0.1 M, pH = 7; prepared by acidification with HCl of a 0.1 M K_2HPO_4 aqueous solution) were used as aqueous electrolytes and $[Co^{III}(NH_3)_5Cl]Cl_2$ (20 mM) as an irreversible electron acceptor in solution. The electrochemical cell was back-illuminated with a 300 W Xenon lamp (Oriel, ozone free). Elimination of IR and UV radiations were performed by a water-filled liquid filter (Spectra-Physics 6123NS) and a cut-off UV-filter (Spectra-Physics 59472 $\lambda > 400$ nm), respectively. Irradiance at the dye-sensitized NiO electrode was measured with a power-meter (Newport PM1918-R) and adjusted to 50•mW cm^{-2} (≈ 1 sun) using a 60% optical density filter.

X-ray Photoelectron Spectrometry (XPS)

The analyses were performed with a VersaProbe II spectrometer from Physical Electronics using a high-resolution monochromatic AlKα line X-ray source at 1486.7 eV. Fixed analyzer pass energy of 23 eV was used for core level scans leading to an overall energy resolution of 0.6 eV. Survey spectra were captured at pass energy of 117 eV. The photoelectron takeoff angle was 45°, which provided an integrated sampling depth of approximately 5 nm. All spectra were referenced against an internal signal, typically by adjusting the C 1s level peak at a binding energy of 284.8 eV.

Surface Mass Spectrometry Analysis (ToF-SIMS)

Time-of-Flight Secondary Ion Mass Spectrometry (ToF-SIMS) measurements were carried out on a TRIFT III ToF-SIMS instrument from Physical Electronics operated with a pulsed 22 keV Au^+ ion gun (ion current of 2nA) rastered over a 300 μm x 300 μm area. An electron gun was operated in pulsed mode at low electron energy for charge compensation. Ion dose was kept below the static conditions limit. Data were analyzed using the WinCadence software. Mass calibration was performed on hydrocarbon secondary ions.

Time-resolved Fluorescence Measurements

The setup for emission lifetime measurements of ruthenium complexes both in solution and grafted onto NiO film has been described previously.53 A Hamamatsu HPDTA streak camera in concert with a Ti:sapphire laser (Tsunami, Newport Spectra-Physics GmbH) was used. To record emission, the repetition rate of the laser was reduced to 400 kHz using a pulse selector (Model 3980, Newport Spectra-Physics GmbH) and the fundamental output of the oscillator was frequency doubled to yield 390 nm pump pulses. For dye-sensitized NiO films, the sample was placed in aca. 60° angle with respect to the excitation beam and emission light is collected from the front side of the sample in a 90° geometry. The emission spectra of ruthenium complexes both in solution and grafted onto NiO films were recorded at wavelengths between 580 and 720 nm.

Femtosecond Transient Absorption Measurements

The setup for transient absorption measurement of ruthenium complex both in solution and grafted onto NiO films has been described previously.54–56 Pump pulses to excite the

sample were centered at 480 nm and the pump-pulse energy was adjusted to 1.2 μJ, while typical probe intensities fall into the range of hundred nJ. The mutual polarizations of pump and probe set to the magic angle. The time resolution of the experiment was characterized by a 150 fs FWHM (full width at half maximum) of the cross correlation function at the fundamental 800 nm and 480 nm. For a kinetic analysis the differential optical density data was chirp corrected and subsequently subjected to a global fit routine using a sum of exponentials for data analysis.57 To avoid prominent contributions from coherent artifacts, 58,59 the pulse overlap region (±150 fs around time zero) was excluded in the data fitting procedure. To avoid sample degradation the sample was moved during individual pump-probe experiments. Sample integrity was ensured by measuring the steady-state absorption spectra prior to and post each measurement.

Results and discussion

Synthesis and characterization of the ruthenium photosensitizers

Phosphonic acids are well-known to form robust monolayers on transparent conducting oxides through covalent reaction with surface hydroxyl groups60–62 and to display excellent grafting stability,62 especially in the aqueous medium required for DS-PEC applications.10,49,63 Ruthenium tris-diimine complexes varying either by the number of methylphosphonic acid anchoring groups – two or four, or by the nature of the third diimine N^N ligand (N^N = bipyridine (bpy) or dipyridophenazine (dppz)) were selected in this study. **RuP_2^{OEt}-bpy** (Figure 1) was prepared by reaction of commercially available $[Ru(bpy)_2Cl_2]$ with the 4,4′-bis(diethylphosphonomethyl)-2,2′-bipyridine ligand (4,4′-$(CH_2PO_3Et_2)_2$-bpy), as previously described.49 **RuP_4^{OEt}-bpy** and **RuP_4^{OEt}-dppz** (Figure 1) were synthesized according to the following two-step procedure recently reported by S. Rau and co-workers:64 first, reaction of $[Ru(dmso)_4Cl_2]$ with two equivalents of 4,4′-$(CH_2PO_3Et_2)_2$-bpy yielded the mixture of complexes $[Ru(4,4'\text{-}(CH_2PO_3Et_2)_2\text{-}bpy)_2Cl_{2-x}(dmso)_x]Cl_x$, which is not purified and directly reacted with the desired N^N ligand to efficiently afford the $[Ru(4,4'\text{-}(CH_2PO_3Et_2)_2\text{-}bpy)_2(N^N)](PF_6)_2$ complexes.

Photophysical and electrochemical properties

The UV/vis absorption and emission spectra of **RuP_2^{OEt}-bpy**, **RuP_4^{OEt}-bpy** and **RuP_4^{OEt}-dppz** were recorded in acetonitrile and compared to the parent compounds $[Ru(bpy)_3](PF_6)_2$ and $[Ru(bpy)_2(dppz)](PF_6)_2$ (Figures S1 and S2 in Supporting Information). Spectroscopic data are summarized in Table 1. These are typical for ruthenium polypyridyl complexes, with intense absorption bands around 300 nm, attributed to ligand-centered π-π* transitions; **RuP_4^{OEt}-dppz** displays an additional band at 358 nm attributed to a dppz-centered transition.65 The visible part of the spectrum is dominated by the classical metal-to-ligand charge-transfer (MLCT) transition centered on 450 nm. In comparison to the parent $[Ru(bpy)_3](PF_6)_2$, the functionalization of bpy with weak electron-donating methyl phosphonate anchoring groups both in **RuP_2^{OEt}-bpy** and **RuP_4^{OEt}-bpy** causes a slight bathochromic shift of the MLCT bands, *i.e.* 0.01 – 0.04 eV, due to stabilization of bpy-based π* orbital. Analogous bathochromic shift of the MLCT bands is also observable in **RuP_4^{OEt}-dppz** compared to $[Ru(bpy)_2(dppz)](PF_6)_2$.

All ruthenium complexes investigated here are weakly emissive with quantum yields of 2.9, 2.0 and 4.1% for **RuP_2^{OEt}-bpy**, **RuP_4^{OEt}-bpy** and **RuP_4^{OEt}-dppz**, respectively. Upon excitation at 495 nm, **RuP_2^{OEt}-bpy** and **RuP_4^{OEt}-bpy** exhibit emission with maximum intensity at 625 nm, close to the parent $[Ru(bpy)_3](PF_6)_2$ (627 nm). Meanwhile, emission maximum of **RuP_4^{OEt}-dppz** is red-shifted at 646 nm, implying that the ^{3}MLCT emissive state is most probably localized on the dppz ligand, which is lower in energy than the bpy one. In addition, the excited-states are characterized by lifetimes of 174, 197 and 192 ns for **RuP_2^{OEt}-bpy**, **RuP_4^{OEt}-bpy**, and **RuP_4^{OEt}-dppz**, respectively (Figure S3 in Supporting Information).

Electrochemical characterization of complexes **RuP_2^{OEt}-bpy**, **RuP_4^{OEt}-bpy** and **RuP_4^{OEt}-dppz** (Table 1; Figure S4 in Supporting Information) was conducted in degassed acetonitrile solution (0.1 M *n*-Bu_4NBF_4). On the anodic scan, a quasi-reversible one-electron wave can be identified at E_{ox} = +0.87 for **RuP_2^{OEt}-bpy**, **RuP_4^{OEt}-bpy** and +0.89 V *vs* Fc^+/Fc for **RuP_4^{OEt}-dppz**. By analogy to previous reports on related polypyridyl ruthenium complexes,49,66 this couple can be unambiguously assigned to the metal-centered $Ru^{III/II}$ process. On the cathodic scan, the cyclic voltammograms of complexes **RuP_2^{OEt}-bpy** and **RuP_4^{OEt}-bpy** show three quasi-reversible one-electron reductions, assigned to successive reductions of the three diimine ligands (bpy and 4,4´-$(CH_2PO_3Et_2)_2$-bpy). In addition, **RuP_4^{OEt}-dppz** displays an additional reductive event at -1.35 V *vs* $Fc^{+/0}$, assigned to the pyrazine-based reduction on the dppz ligand, in comparison to the parent compound $[Ru(bpy)_2(dppz)](PF_6)_2$.67 Overall, the electronic properties of the three photosensitizers are not significantly modified by the introduction of either two or four methylphosphonate substituents on the bpy ligands, in agreement with the methylene group acting as an electronic insulator between the bpy ligand and the phosphonic acid anchoring group.38

NiO film sensitization and characterization

The phosphonic acid derivatives **RuP_2^{OH}-bpy**, **RuP_4^{OH}-bpy** and **RuP_4^{OH}-dppz** were prepared by acidic hydrolysis of complexes **RuP_2^{OEt}-bpy**, **RuP_4^{OEt}-bpy** and **RuP_4^{OEt}-dppz**.74 We previously reported ITO-75 and NiO-based52 photocathodes sensitized with **RuP_2^{OH}-bpy**. According to these studies,52,75 film sensitization was performed by soaking the films for 24 hours under orbital stirring in a 50 μM methanolic solution of the desired complex. Commercially available NiO film preparation, previously shown to display one of the highest photoelectrochemical performances in our joint benchmarking study,36 was selected here.

Surface modification by the molecular ruthenium complexes was confirmed by X-ray Photoelectron Spectroscopy (XPS) and Time-of-Flight Secondary Ion Mass Spectrometry (ToF-SIMS). The survey high resolution XPS spectra of the different NiO films are shown in Figure S5, together with a blank NiO film analyzed for comparison purpose. The chemical composition of the latter is in excellent agreement with previously reported XPS studies.76,77 These features are not modified upon sensitization with either **RuP_2^{OH}-bpy**, **RuP_4^{OH}-bpy** or **RuP_4^{OH}-dppz**. In addition, new peaks are observed at 132.6 eV, 399.8 eV and 462.8 eV, characteristics for P_{2p}, N_{1s} and $Ru_{3p3/2}$ core levels respectively (Figure S6 in Supporting Information).

The highly sensitive ToF-SIMS technique was also employed to probe the films extreme surface in order to provide more mass-related molecular information. Spectra acquired in the positive mode exhibit numerous signatures of ruthenium-containing ions (see Figure S7 and Table S1 in Supporting Information), easily identified thanks to the Ru specific isotopic pattern. Two major fragmentation pathways are identified: the first one involves diimine ligand decoordination, as previously observed for $Ru(bpy)_3$-electrografted monolayers onto glassy carbon78 (for instance, peaks detected at m/z = 414 ($[Ru(bpy)_2]^+$), 257 ($[Ru(bpy)]^+$) and 157 ($bpyH^+$) for **NiO|RuP$_2$-bpy**); the second fragmentation pathway proceeds through breaking of the CH_2-P bond in these phosphonate-substituted entities (for instance, peaks detected at m/z = 438 ($[Ru(bpy)(bpy(CH•)(CH_2•))]^+$) for **NiO|RuP$_2$-bpy** and **NiO|RuP$_4$-bpy**, at m/z = 563 ($[Ru(dppz)(bpy(C•)(CH_2•))]^+$) for **NiO|RuP$_4$-dppz**). Of note, the highest intensity ruthenium-containing secondary ions contain the non-substituted ligand (bpy or dppz), which enable a clear identification of each grafted dye; moreover, the phosphonate-substituted bpy ligand is never detected intact (without fragmentation), which fully supports a chemisorption rather than a physisorption process. In addition, spectra recorded in the negative mode provide further evidence for the covalent nature of the grafting of Ru complexes to NiO: various $Ni_aP_bO_cH_d^-$ fragments (such as those detected at m/z = 138 ($NiPO_3H^-$), 154 ($NiPO_4H^-$), 200 ($Ni_2P_2O_5^-$) and 216 ($Ni_2P_2O_6^-$)) were identically detected for the three functionalized NiO films, compared to a blank sample (Figure S8 in Supporting Information); this clearly demonstrates the formation of strong P–O–Ni bonds at the surface of the NiO films, as similarly reported for phosphonic acid monolayers onto TiO_2 films.79,80 Finally, ToF-SIMS allows for a chemical mapping and it was checked that high mass peaks characteristic to the grafted dyes do not exhibit any heterogeneous distribution (Figure S9 in Supporting Information), at least at the lateral resolution obtained in the high mass resolution acquisition mode (estimated to a few microns).

Film sensitization was further quantified by UV visible absorption spectroscopy (Figures 2 and S10 in Supporting Information). After subtraction of the blank NiO film absorption, the dye-sensitized electrodes spectra display absorption features in the visible region, characteristic for the MLCT transition of the grafted ruthenium polypyridyl photosensitizers, as shown in Figure 2 for **NiO|RuP$_4$-dppz**.

As previously reported,52,75,81 surface concentrations were estimated using the following equation (assuming that the molar absorption coefficients ε of the dyes are not modified upon hydrolysis and grafting64):

$$surf.conc.\left(mol.cm^{-2}\right)=\frac{Abs_{\max}}{1000\,x\,\varepsilon_{\max}\left(M^{-1}.cm^{-1}\right)} \quad \text{(eq. 1)}$$

Surface concentrations of 16.1 ± 3.5 nmol.cm^{-2} and 13.7 ± 0.8 nmol.cm^{-2} (average out of 8 samples) were estimated for **RuP$_4^{OH}$-bpy** and **RuP$_4^{OH}$-dppz**, respectively, which is roughly twice more than **RuP$_2^{OH}$-bpy** (8.7 ± 2.3 nmol.cm^{-2}); this increased grafting efficiency can be directly correlated to the presence of four anchoring groups on the former photosensitizers. Surface concentration determination for related ruthenium tris diimine-sensitized NiO films is only scarcely reported in the literature. We previously reported the

grafting of **RuP_2^{OH}-bpy** onto PS-*b*-P2PV-templated NiO films with a surface coverage of 1.5-2.8 nmol.cm^{-2}.52 Using the same photosensitizer, Odobel and co-workers calculated a maximum surface coverage of 1.2 μmol.m^{-2} (equivalent to 0.12 nmol.cm^{-2}) from Langmuir isotherm plots.38 Finally, a maximum surface loading in the range of 30 nmol.cm^{-2} was obtained by Y. Wu and co-workers for cyclometallated ruthenium sensitizers bearing two carboxylate anchoring groups.42 It is important to highlight that the amount of dye loading is strongly dependent on the NiO film preparation,36 on its thickness and on the nature of the anchoring groups,38 which prevents any straightforward comparison.

Photoelectrochemical properties of dye-sensitized NiO films

Most of the studies dealing with the grafting of Ru complexes onto NiO assess their photovoltaic performances in acetonitrile,38,40–42 and are thus of limited interest for water splitting applications. Here, the spectroelectrochemical properties of the dye-sensitized NiO films were assessed by chronoamperometric measurements in fully aqueous medium, applying a potential of 0 V vs Ag/AgCl in the presence of 20 mM of $[Co^{III}(NH_3)_5Cl]Cl_2$, used as an irreversible electron acceptor (IEA).52,75 Upon reduction, this complex irreversibly decomposes into $[Co^{II}(H_2O)_6]^{2+}$, thus limiting recombination in the electrode diffusion layer. The Gibbs free energies were determined for both hole injection from the excited dye into the NiO valence band (ΔG_{inj}) and electron transfer from the reduced dye to the IEA (*i.e.* dye regeneration; ΔG_{reg}); these two processes are exergonic for the three dyes (Table 1), which is favourable for photocurrent generation. Indeed, upon visible light irradiation of the dye-sensitized NiO electrodes, cathodic photocurrents build up (Figure 3), ascribed to the establishment of photoinduced electron transfers from the NiO valence band to IEA, mediated by the excited state of the photosensitizer (Figure 3A).

For each dye-sensitized electrode, the measurements were carried out first in acetate buffer (pH 4.5), then in phosphate buffer (pH 7), under chopped light irradiation (visible light; 50 mW.cm^{-2}). Higher photocurrent densities were, in the three cases, recorded at pH 7, although the difference is faint for **NiO|RuP_4-dppz**: macroscopic photocurrents as high as 170 μA.cm^{-2} (pH 4.5) and 190 μA.cm^{-2} (pH 7) were indeed obtained, in the same range than those we previously described with a push-pull organic dye.52 In the absence of IEA in solution, small cathodic photocurrents were recorded (≈ 35 μA.cm^{-2} for **NiO|RuP_4-dppz**, see Figure S11 in Supporting Information), as previously observed52 and tentatively attributed to the reduction of residual traces of oxygen trapped within the nanostructured surface of the dye-sensitized electrode.82 Furthermore, non-sensitized NiO electrodes do not display any photocurrent in the presence of 20 mM of IEA (either at pH 4.5 or pH 7, Figure S12 in Supporting Information), confirming that the ruthenium photosensitizers are at the origin of the observed photoelectrochemical activity.

In order to evaluate the intrinsic efficiency of each photosensitizer to mediate photoinduced electron transfers, comparison needs to be made by taking into account the amount of grafted dye *i.e.* by dividing the photocurrent density (*j*) by the surface coverage (Γ, estimated by UV/vis absorption measurements). Although displaying a significantly lower driving force ΔG_{reg} (Table 1), **RuP_4-dppz** is the most efficient photosensitizer of the series, with an activity 1.5 to 2 times higher in ascorbate buffer, pH 4.5 (12.1 μA.nmol^{-1}.cm^{-2}) than the ones

obtained for **RuP_4-bpy** (7.9 μA.nmol^{-1}.cm^{-2}) and **RuP_2-bpy** (5.6 μA.nmol^{-1}.cm^{-2}), respectively (see Table 2). This result indicates that the specific charge transfer properties of the dppz ligand dominate over other parameters to control photocurrent generation; the electron in the reduced **RuP_4-dppz** is indeed localized on the phenazine moiety, which means at an increased distance from the NiO surface compared to the other reduced dyes. This could make it more accessible for reaction with the electrolyte and also slow down charge recombination, as previously reported for related systems.41 The later point will be studied and discussed in more details in the next section.

Finally, these measurements brought some preliminary information about the stability of the dye-sensitized NiO films under such aqueous working conditions, relevant for DS-PEC applications. Apart for the **RuP_4-dppz** sensitized electrode at pH 4.5 (discussed below), a small decrease in the photocurrent density is observed during the first three irradiation cycles, while the photocurrent density then stabilizes for the next cycles. This behavior can be tentatively assigned to some surface reorganization at the beginning of the experiment. No drastic pH effect is observed, 80 to 90 % of the photocurrent density being maintained at pH 4.5 just as pH 7. By contrast, no loss of activity at all is observed for **NiO|RuP_4-dppz** in acetate buffer pH 4.5, a behavior that we previously observed with a push-pull organic dye. 52 Other parameters vary in addition to the pH value: nature of the buffer, solubility of the grafted dye… The good stability of **NiO|RuP_4-dppz** may be due to a combined effect of a lower water solubility and a lower competition for NiO surface binding of the acetate buffering species. Although a more detailed and systematic analysis of the stability of these dye-sensitized electrodes would be required for a deep understanding of their behavior under photoelectrochemical conditions, **RuP_4-dppz** combines the highest photocurrents of the series with good stability at pH 4.5, pH of activity of various cobalt-based H_2-evolving catalysts.52,83–86 This last result is particularly interesting in the context of DS-PEC applications.

Time-resolved Absorption and Emission Spectroscopies

Ultrafast transient absorption and time-resolved emission measurements were carried out to elucidate the hole injection and recombination dynamics of the series of ruthenium complexes on NiO films. These photoinduced elementary processes are mechanistically essential for photocurrent generation in photoelectrochemical device. To aid the discussion of the data obtained for the sensitized NiO films, transient absorption of the complexes were recorded first in acetonitrile solution with excitation at 480 nm (Figure S13 in Supporting Information). The data recorded are in agreement with literature reports on the parent complexes,87,88 which do not carry any methyl phosphonate groups, again revealing that introduction of the anchoring groups does not significantly affect the chromophoric properties: the data for **RuP_2^{OEt}-bpy** and **RuP_4^{OEt}-bpy** exhibit a broad and structureless excited-state absorption (ESA), without any ground-state bleaching (GSB) within the experimentally accessible probe window. This structureless ESA can be assigned to the absorption of the ^{3}MLCT excited state, attributed to ligand-to-metal (bpy-π –> metal-dπ) charge transfers.89 Interestingly, 95% of the initial ESA signal remains within the experimental time window (~ 1.8 ns) for both complexes (Figure S14 in Supporting Information). This is indicative of the population of a long-lived ^{3}MLCT excited state,

typical for Ru tris-bipyridine complexes. The transient absorption spectrum of **RuP_4^{OEt}-dppz** reveals different spectral features compared to **RuP_2^{OEt}-bpy** and **RuP_4^{OEt}-bpy**. Indeed, GSB is observed at 500 – 520 nm and is progressively blue-shifted over increasing delay times. A broad ESA, peaking at 580 nm, can also be identified. This absorption band increases in intensity over the first 100 ps after photoexcitation and subsequently decays by approximately 20%. A long-lived ^{3}MLCT excited state is also found in **RuP_4^{OEt}-dppz**, as previously observed for other dppz-containing Ru complexes.57,90

Transient absorption data obtained for the complexes grafted on NiO indicate electronic interaction between the complexes and the surface of NiO (see Figure S15 for raw data). Figure 4a,c,e display the transient absorption spectra of **NiO|RuP_2-bpy**, **NiO|RuP_4-bpy** and **NiO|RuP_4-dppz** photoelectrodes upon excitation at 480 nm, the corresponding kinetic traces at selected probe wavelengths being shown in Figure 4b,d,f. The spectra are characterized by a GSB below 550 nm and a positive, broad positive absorption features at higher wavelengths. It can be noted that the point of zero differential absorption (ΔOD = 0) of the immobilized complexes is shifted to longer probe-wavelengths compared to the isolated complexes in solution. With increasing time delay, the zero absorption difference is dynamically blue-shifted and the ground state bleach at 500 nm is almost completely recovered within the accessible temporal window. This feature indicates that both relaxation of the excited-state and interfacial charge transfer take place.44

The broad positive absorption difference at around 660 nm is associated with the **π-π*** absorption of bipyridine radical anion ($bpy^{\bullet -}$), as also obtained from electrochemically reduced ruthenium-bipyridine complexes.40,43,91 Accordingly, the decay of positive absorption difference at 660 nm synchronized with the recovery of GSB at 550 nm can be ascribed to the formation of charge separated states as a result of hole injection from excited dye into NiO.41,49 This hole injection forms a charge separated state, which is an indispensable intermediate in obtaining high cathodic photocurrents from the molecular-functionalized NiO electrodes. Hole injection in the molecular-functionalized NiO electrodes is further confirmed by time-resolved emission measurements, which are depicted in Figure 5. The data reveals that the emission of the complexes, which is rather long-lived in solution, becomes rapidly quenched on the NiO surface. In agreement with literature, this finding is associated with photoinduced hole injection from the complex into the NiO.44

To quantitatively analyze the hole injection and recombination kinetics, a tri-exponential function with an offset reflecting the respective long-lived component was applied to globally fit the transient absorption data. The resulting decay associated spectra (DAS) of **NiO|RuP_2-bpy**, **NiO|RuP_4-bpy** and **NiO|RuP_4-dppz** are shown in Figure S16 (Supporting Information) and the characteristic time constants are summarized in Table 3. The ultrafast component τ_1 of ~200 fs is interpreted as contributions from ^{1}MLCT→^{3}MLCT intersystem crossing (ISC, typical for this type of complexes) and intramolecular vibrational redistribution, and – likely –fast hole injection into NiO (for **NiO|RuP_4-bpy**, see below). The spectral features associated with τ_2 = 5.8 ps (**NiO|RuP_2-bpy**) and 19.5 ps (**NiO|RuP_4-dppz**) are qualitatively similar to that found in a related system.44 The negative ΔOD signal at 550 nm, i.e. adjacent to the ground-state bleach towards 550 nm, reflect that hole injection from the excited state of **RuP_2-bpy** and **RuP_4-dppz**40,92 to NiO contributes to the observed

processes. This is due to the fact that at around 530 nm both oxidized Ni-centers41,44,93 and reduced Ru^{II} polypyridine sensitizers contribute to the differential absorption signal.89 Although the injection rates in **NiO|RuP$_2$-bpy** and **NiO|RuP$_4$-dppz** estimated here are slower than the rates observed in most organic dye-sensitized NiO electrodes (hundreds of fs to ~1 ps),94–96 these values are comparable to those found in other studies related to ruthenium photosensitizers.43,44

Comparing the DAS of the some-ps components of **NiO|RuP$_2$-bpy** and **NiO|RuP$_4$-dppz** to **NiO|RuP$_4$-bpy**, it becomes apparent that the latter does only reveal a very minor negative ΔOD structure adjacent to the ground-state bleach (see red shift of the 6.1 ps component compared to the long-lived component). This feature is however associated with oxidized Ni-centers and reduced Ru^{II} sensitizer, i.e. hole injection into the semiconductor. Recalling that cathodic photocurrents were observed for **NiO|RuP$_4$-bpy** (see Figure 3), it is concluded that in this system dominant parts of the ultrafast hole injection occur beyond the time-resolution of the spectroscopic experiment. Apparently increasing the number of anchoring groups increases the likelihood that right upon photoexcitation an electronic state is populated, which is highly prone to hole injection. Along these lines, the 6.1 ps component in **NiO|RuP$_4$-bpy** might be assigned to some vibrational relaxation occurring after formation of the reduced **RuP$_4$-bpy**.97,98

τ_3 reflects a process in which ground state bleach decays without contributions from products of hole injection building up. Hence, τ_3 is assigned to charge recombination (*vide infra*). The magnitude and the spectral contributions, i.e. the decay associated spectra, associated with τ_3 are rather similar for all ruthenium complexes on NiO. This indicates that the process associated with τ_3 stems from charge recombination *irrespective of the specific molecular structure*. During the ultrafast photoinduced dynamics, the intensity of the ESA band integrated between 650 and 700 nm decays by 63%, 71% and 43% for **NiO|RuP$_2$-bpy**, **NiO|RuP$_4$-bpy**, **NiO|RuP$_4$-dppz**, respectively. These numbers are derived based on the integrated ESA intensity recorded at the longest delay times relative to the maximal signal amplitude of the ESA band recorded at 150 fs after photoexcitation. However, it should be noted that the charge recombination associated with τ_3 is only partial as a long-lived (on the time window of the experiment) component is observable in the data. These findings are in line with literature, which reports that in the absence of a redox mediator (as in our measurements) recombination kinetics leading to a decay of the interfacial charge-separated state of NiO(+)-Ru^{II}-bpy(-) are characterized with time constants of up to 5 μs.40,41,43 Hence, such slow recombination processes will occur at long-time offsets in our differential absorption data and only the partial sub-ns recombination kinetics are visible in the experiments performed here.

The photophysical model, which summarizes the observations of the ultrafast spectroscopy, is presented in Figure 6. The model is based on the notion that the substitution of the bpy ligands by the anchoring groups does not significantly disturb the chromophoric properties of the **RuP$_2$-bpy** and **RuP$_4$-bpy** complexes, compared to $[Ru(bpy)_3]^{2+}$. Thus, upon light absorption the electron density is quasi equally distributed over the three bpy ligands. However, upon fast hole injection, two distinct electronic configurations become possible, i.e. one in which a bpy ligand bearing the phosphonate anchoring groups is reduced and

another one in which the unsubstituted bpy ligand is reduced. In case the radical anion is formed on a phosphonate-substituted anchoring ligand, relatively fast charge recombination is observed, i.e. the process associated with τ_3. On the contrary, if the electron is localized on the non-substituted bpy ligand, i.e. more decoupled from the NiO surface, the kinetics of recombination is slowed down, giving rise to the long-lived component observed in our transient absorption data. This shows that even by as little modifications as asymmetrically substituting a $Ru(bpy)_3$ core with anchoring groups, a molecular push-pull effect can be achieved.44

Discussion of results from time-resolved spectroscopy in relation to the observed macroscopic photoelectrochemical activity

All complexes investigated here to sensitize NiO films reveal sizeable photocurrents under the chosen experimental conditions. The magnitude of the photocurrents scale in the following order (see Table 2): **NiO|RuP$_4$-dppz > NiO|RuP$_4$-bpy > NiO|RuP$_2$-bpy**. This trend does not follow the trend of the rate of hole injection into the NiO, which – comparing the characteristic time scales for the slowest observable injection time constant – is **NiO|RuP$_4$-bpy > NiO|RuP$_2$-bpy > NiO|RuP$_4$-dppz**. In all the investigated photocathodes, the fastest recombination kinetics appears with a time-constant of roughly 400 ps in concert with a slow component (which kinetically extends beyond the accessible time-range of our experiment). By contrast, this slowest recombination process results in remaining ESA intensities (integrated in the spectral region between 650 and 700 nm) at long delay times of 37%, 29% and 57% for **NiO|RuP$_2$-bpy**, **NiO|RuP$_4$-bpy** and **NiO|RuP$_4$-dppz** of the ESA amplitude right after photoexcitation, respectively. It is thus tempting to correlate the differences in the observed photocurrents with the differences in the recombination behavior of the charge-separated states. Such long-lived components (> 3 ns) have also been previously observed for related ruthenium tris-diimine sensitized NiO films,40,43,44 but they represented relatively smaller fractions of the ESA amplitude, for instance 4 to 13 % in the study by Wu and coworkers.40 Conjugated carboxylate anchors were employed in these examples, which are known to strongly modify the electronics of the ligand.44,99 We specifically selected non-conjugated methyl phosphonate functions and we show in this study that they do not modify the properties of the $Ru(bpy)_3$ chromophore; we believe this could account for the increased weight of this long-lived charge separated state.

To definitely relate this long-lived charge separated state to photocurrent generation, we need to also consider its subsequent reaction with the IEA. The electron transfer reaction from the reduced dye anchored at the NiO surface to the irreversible electron acceptor is controlled by diffusion of the IEA in the electrolyte. It thus occurs – at fastest – on a nanosecond timescale, and hence it would match the lifetime estimated for the long-lived charge separated state. Second, photoelectrochemical measurements are carried out at an applied potential of 0 V *vs* Ag/AgCl. A dependency between the potential applied to the NiO electrode and the charge recombination rate was recently reported by Hammarström and coworkers, from ns timescale measurements made at different applied potentials on NiO films sensitized with a ruthenium tris diimine-based dyad.48 According to this study, the NiO band gap states should be almost completely filled with electrons at the applied potential of 0 V *vs* Ag/AgCl (–0.343 V *vs* $Ag/AgNO_3$ for comparison with the reported

study). With holes rapidly removed from the valence band via the conductive substrate, the reduced dyes formed with our three systems should be greatly stabilized (recombination strongly disfavored); as a consequence, diffusion-controlled reaction with the IEA would be even more favored, in agreement with the photocurrents measured for the three electrodes. This efficient hole collection at the back FTO conductive layer also prevents nickel hydroxide formation at the electrode – aqueous electrolyte interface; the latter was observed during electrochemical oxidation of NiO films at a more positive applied potential and led to a deleterious NiO dissolution into the electrolyte.100

Furthermore, when considering the relative amplitudes of the individual kinetic components as obtained from the global fit, it becomes apparent that for **NiO|RuP$_2$-bpy** and **NiO|RuP$_4$-bpy** the weights of the processes associated with τ_3 and the infinite component amount to roughly 60% (see Table 2), while for **NiO|RuP$_4$-dppz** these two components account for about 75% of the overall decay. This implies that for the sensitizer bearing the dppz-ligand the charge separated state becomes stabilized, likely due to the interplay of phenazine and phenantroline based electronic states, which are both accessible in this structure. The specific electronic and geometrical structure of the dppz-ligand101,102 allows for excess electron density to be moved away from the anchoring ligands and hence the weight of the long-lived component is strongly increased compared to the one for **NiO|RuP$_4$-bpy**, bearing the same number of anchoring groups. This stabilized charge-transfer state in turn leads to much higher photocurrents in the presence of sacrificial electron acceptors, as observed with the **RuP$_4$-dppz** sensitizer compared to the bpy-based ones.

Conclusions

The study presented in this paper compares the spectroscopic properties and the photoelectrochemical activities of NiO photocathodes sensitized by ruthenium tris-diimine complexes varying by the number of anchoring groups and by the nature of the third ligand. ToF-SIMS was successfully employed to provide mass-related molecular information for the grafted species and to confirm their chemisorption through Ni-O-P bonds. Cathodic photocurrents intensities up to 190 μA.cm^{-2} were generated in fully aqueous medium upon visible light irradiation in the presence of an irreversible electron acceptor. In addition, femtosecond transient absorption spectroscopy gave access to the kinetic parameters associated with hole injection and charge recombination. The latter is shown to occur over a wide range of timescales, as also recently reported for an organic-dye sensitized NiO electrode.47

Our results establish that (i) increasing the number of anchoring groups from two to four is important to improve the grafting efficiency; (ii) by contrast with the previously reported conjugated carboxylate anchors, substitution of the Ru(bpy)$_3$ and Ru(bpy)$_2$(dppz) cores by two or four methylphosphonate anchors does not modify the electronic properties of the dye; this property is the basis for the photophysical model proposed here; (iii) additionally, substituting a π-accepting dppz for the bpy ligand stabilizes the charge-separated state, in agreement with the much larger signal remaining on the ns timescale. The higher relative amplitude of the long-lived charge-separated state for **NiO|RuP$_4$-dppz**, compared to the bpy-based photoelectrodes, provides a rational for the higher photocurrent intensities. In the

future and before their integration into functional water splitting devices, characterization of such dye-sensitized photocathodes by transient absorption studies at different timescales – from fs to μs – and with an applied potential will be required for a complete understanding of their performances.

Supporting Information

Refer to Web version on PubMed Central for supplementary material.

Acknowledgment

This work was supported by the French National Research Agency (PhotoCAT project – ANR-14-JTIC-0004-01 and the Labex program ARCANE – ANR-11-LABX-0003-01), the European Research Council under the European Union's Seventh Framework Program FP/2007-2013 (ERC Grant Agreement n.306398 and COST Action CM1202 PERSPECT-H_2O) and the German Academic Exchange Service (DAAD) for financial support.Colette Lebrun (CEA, INAC−SCIB), M. W. Daniela and Jean-François Lefebvre (LCBM) are acknowledged for the ESI-MS, the synthetic support and some fluorescence measurements, respectively.

References

(1). Brennaman MK, Dillon RJ, Alibabaei L, Gish MK, Dares CJ, Ashford DL, House RL, Meyer GJ, Papanikolas JM, Meyer TJ. Finding the Way to Solar Fuels with Dye-Sensitized Photoelectrosynthesis Cells. J Am Chem Soc. 2016; 138:13085–13102.

(2). Queyriaux N, Kaeffer N, Morozan A, Chavarot-Kerlidou M, Artero V. Molecular cathode and photocathode materials for hydrogen evolution in photoelectrochemical devices. J Photochem Photobiol C. 2015; 25:90–105.

(3). Ashford DL, Gish MK, Vannucci AK, Brennaman MK, Templeton JL, Papanikolas JM, Meyer TJ. Molecular Chromophore–Catalyst Assemblies for Solar Fuel Applications. Chem Rev. 2015; 115:13006–13049. [PubMed: 26513130]

(4). Yu Z, Li F, Sun L. Recent advances in dye-sensitized photoelectrochemical cells for solar hydrogen production based on molecular components. Energy Environ Sci. 2015; 8:760–775.

(5). Odobel F, Pellegrin Y. Recent Advances in the Sensitization of Wide-Band-Gap Nanostructured p-Type Semiconductors. Photovoltaic and Photocatalytic Applications. J Phys Chem Lett. 2013; 4:2551–2564.

(6). Li F, Fan K, Xu B, Gabrielsson E, Daniel Q, Li L, Sun L. Organic Dye-Sensitized Tandem Photoelectrochemical Cell for Light Driven Total Water Splitting. J Am Chem Soc. 2015; 137:9153–9159. [PubMed: 26132113]

(7). Hagfeldt A, Boschloo G, Sun L, Kloo L, Pettersson H. Dye-Sensitized Solar Cells. Chem Rev. 2010; 110:6595–6663. [PubMed: 20831177]

(8). Grätzel M. Dye-sensitized solar cells. J Photochem Photobiol C. 2003; 4:145–153.

(9). O'Regan B, Gratzel M. A low-cost, high-efficiency solar cell based on dye-sensitized colloidal TiO_2 films. Nature. 1991; 353:737–740.

(10). Pechy P, Rotzinger FP, Nazeeruddin MK, Kohle O, Zakeeruddin SM, Humphry-Baker R, Gratzel M. Preparation of phosphonated polypyridyl ligands to anchor transition-metal complexes on oxide surfaces: application for the conversion of light to electricity with nanocrystalline TiO_2 films. J Chem Soc Chem Commun. 1995:65–66.

(11). Younpblood WJ, Lee SHA, Kobayashi Y, Hernandez-Pagan EA, Hoertz PG, Moore TA, Moore AL, Gust D, Mallouk TE. Photoassisted Overall Water Splitting in a Visible Light-Absorbing Dye-Sensitized Photoelectrochemical Cell. J Am Chem Soc. 2009; 131:926–927. [PubMed: 19119815]

(12). Brimblecombe R, Koo A, Dismukes GC, Swiegers GF, Spiccia L. Solar driven water oxidation by a bioinspired manganese molecular catalyst. J Am Chem Soc. 2010; 132:2892–2894. [PubMed: 20155923]

(13). Bard AJ. Inner-Sphere Heterogeneous Electrode Reactions. Electrocatalysis and Photocatalysis: The Challenge. J Am Chem Soc. 2010; 132:7559–7567. [PubMed: 20469860]

(14). Song W, Glasson CRK, Luo H, Hanson K, Brennaman MK, Concepcion JJ, Meyer TJ. Photoinduced Stepwise Oxidative Activation of a Chromophore–Catalyst Assembly on TiO_2 . J Phys Chem Lett. 2011; 2:1808–1813.

(15). Moore GF, Blakemore JD, Milot RL, Hull JF, Song H-e, Cai L, Schmuttenmaer CA, Crabtree RH, Brudvig GW. A visible light water-splitting cell with a photoanode formed by codeposition of a high-potential porphyrin and an iridium water-oxidation catalyst. Energy Environ Sci. 2011; 4:2389–2392.

(16). Zhao Y, Swierk JR, Megiatto JD, Sherman B, Youngblood WJ, Qin D, Lentz DM, Moore AL, Moore TA, Gust D, Mallouk TE. Improving the efficiency of water splitting in dye-sensitized solar cells by using a biomimetic electron transfer mediator. Proc Natl Acad Sci USA. 2012; 109:15612–15616. [PubMed: 22547794]

(17). Ashford DL, Song W, Concepcion JJ, Glasson CRK, Brennaman MK, Norris MR, Fang Z, Templeton JL, Meyer TJ. Photoinduced Electron Transfer in a Chromophore–Catalyst Assembly Anchored to TiO_2. J Am Chem Soc. 2012; 134:19189–19198. [PubMed: 23101955]

(18). Xiang X, Fielden J, Rodríguez-Córdoba W, Huang Z, Zhang N, Luo Z, Musaev DG, Lian T, Hill CL. Electron Transfer Dynamics in Semiconductor–Chromophore–Polyoxometalate Catalyst Photoanodes. J Phys Chem C. 2013; 117:918–926.

(19). Gao Y, Ding L, Liu J, Wang L, Lu Z, Li L, Sun L. Visible Light Driven Water Splitting in a Molecular Device with Unprecedentedly High Photocurrent Density. J Am Chem Soc. 2013; 135:4219–4222. [PubMed: 23465192]

(20). Alibabaei L, Brennaman MK, Norris MR, Kalanyan B, Song W, Losego MD, Concepcion JJ, Binstead RA, Parsons GN, Meyer TJ. Solar water splitting in a molecular photoelectrochemical cell. Proc Natl Acad Sci USA. 2013; 110:20008–20013. [PubMed: 24277806]

(21). Nayak A, Knauf RR, Hanson K, Alibabaei L, Concepcion JJ, Ashford DL, Dempsey JL, Meyer TJ. Synthesis and photophysical characterization of porphyrin and porphyrin-Ru(II) polypyridyl chromophore-catalyst assemblies on mesoporous metal oxides. Chem Sci. 2014; 5:3115–3119.

(22). Ding X, Gao Y, Zhang L, Yu Z, Liu J, Sun L. Visible Light-Driven Water Splitting in Photoelectrochemical Cells with Supramolecular Catalysts on Photoanodes. ACS Catalysis. 2014; 4:2347–2350.

(23). Gao Y, Zhang L, Ding X, Sun L. Artificial photosynthesis - functional devices for light driven water splitting with photoactive anodes based on molecular catalysts. Phys Chem Chem Phys. 2014; 16:12008–12013. [PubMed: 24658163]

(24). Zhang L, Gao Y, Ding X, Yu Z, Sun L. High-Performance Photoelectrochemical Cells Based on a Binuclear Ruthenium Catalyst for Visible-Light-Driven Water Oxidation. ChemSusChem. 2014; 7:2801–2804. [PubMed: 25139154]

(25). Ashford DL, Sherman BD, Binstead RA, Templeton JL, Meyer TJ. Electro-assembly of a Chromophore–Catalyst Bilayer for Water Oxidation and Photocatalytic Water Splitting. Angew Chem Int Ed. 2015; 54:4778–4781.

(26). Yamamoto M, Wang L, Li F, Fukushima T, Tanaka K, Sun L, Imahori H. Visible light-driven water oxidation using a covalently-linked molecular catalyst-sensitizer dyad assembled on a TiO_2 electrode. Chem Sci. 2016; 7:1430–1439.

(27). Li L, Duan L, Wen F, Li C, Wang M, Hagfeldt A, Sun L. Visible light driven hydrogen production from a photo-active cathode based on a molecular catalyst and organic dye-sensitized p-type nanostructured NiO. Chem Commun. 2012; 48:988–990.

(28). Tong L, Iwase A, Nattestad A, Bach U, Weidelener M, Gotz G, Mishra A, Bauerle P, Amal R, Wallace GG, Mozer AJ. Sustained solar hydrogen generation using a dye-sensitised NiO photocathode/$BiVO_4$ tandem photo-electrochemical device. Energy Environ Sci. 2012; 5:9472–9475.

(29). Ji Z, He M, Huang Z, Ozkan U, Wu Y. Photostable p-Type Dye-Sensitized Photoelectrochemical Cells for Water Reduction. J Am Chem Soc. 2013; 135:11696–11699. [PubMed: 23895560]

(30). Fan K, Li F, Wang L, Daniel Q, Gabrielsson E, Sun L. Pt-free tandem molecular photoelectrochemical cells for water splitting driven by visible light. Phys Chem Chem Phys. 2014; 16:25234–25240. [PubMed: 25341620]

(31). Click KA, Beauchamp DR, Huang Z, Chen W, Wu Y. Membrane-inspired acidically stable dye-sensitized photocathode for solar fuel production. J Am Chem Soc. 2016; 138:1174–1179. [PubMed: 26744766]

(32). Gross MA, Creissen CE, Orchard KL, Reisner E. Photoelectrochemical hydrogen production in water using a layer-by-layer assembly of a Ru dye and Ni catalyst on NiO. Chem Sci. 2016; 7:5537–5546.

(33). Kaeffer N, Massin J, Lebrun C, Renault O, Chavarot-Kerlidou M, Artero V. Covalent design for dye-sensitized H_2-evolving photocathodes based on a cobalt diimine–dioxime catalyst. J Am Chem Soc. 2016; 138:12308–12311. [PubMed: 27595317]

(34). Kou Y, Nakatani S, Sunagawa G, Tachikawa Y, Masui D, Shimada T, Takagi S, Tryk DA, Nabetani Y, Tachibana H, Inoue H. Visible light-induced reduction of carbon dioxide sensitized by a porphyrin–rhenium dyad metal complex on p-type semiconducting NiO as the reduction terminal end of an artificial photosynthetic system. J Catal. 2014; 310:57–66.

(35). Sahara G, Abe R, Higashi M, Morikawa T, Maeda K, Ueda Y, Ishitani O. Photoelectrochemical CO_2 reduction using a Ru(II)-Re(I) multinuclear metal complex on a p-type semiconducting NiO electrode. Chem Commun. 2015; 51:10722–10725.

(36). Wood CJ, Summers GH, Clark CA, Kaeffer N, Braeutigam M, Carbone LR, D'Amario L, Fan K, Farre Y, Narbey S, Oswald F, et al. A comprehensive comparison of dye-sensitized NiO photocathodes for solar energy conversion. Phys Chem Chem Phys. 2016; 18:10727–10738. [PubMed: 26734947]

(37). Odobel F, Pellegrin Y, Gibson EA, Hagfeldt A, Smeigh AL, Hammarström L. Recent advances and future directions to optimize the performances of p-type dye-sensitized solar cells. Coord Chem Rev. 2012; 256:2414–2423.

(38). Pellegrin Y, Le Pleux L, Blart E, Renaud A, Chavillon B, Szuwarski N, Boujtita M, Cario L, Jobic S, Jacquemin D, Odobel F. Ruthenium polypyridine complexes as sensitizers in NiO based p-type dye-sensitized solar cells: Effects of the anchoring groups. J Photochem Photobiol A: Chemistry. 2011; 219:235–242.

(39). Gennari M, Légalité F, Zhang L, Pellegrin Y, Blart E, Fortage J, Brown AM, Deronzier A, Collomb M-N, Boujtita M, Jacquemin D, et al. Long-Lived Charge Separated State in NiO-Based p-Type Dye-Sensitized Solar Cells with Simple Cyclometalated Iridium Complexes. J Phys Chem Lett. 2014; 5:2254–2258. [PubMed: 26279543]

(40). Ji Z, Natu G, Huang Z, Kokhan O, Zhang X, Wu Y. Synthesis, Photophysics, and Photovoltaic Studies of Ruthenium Cyclometalated Complexes as Sensitizers for p-Type NiO Dye-Sensitized Solar Cells. J Phys Chem C. 2012; 116:16854–16863.

(41). Freys JC, Gardner JM, D'Amario L, Brown AM, Hammarstrom L. Ru-based donor-acceptor photosensitizer that retards charge recombination in a p-type dye-sensitized solar cell. Dalton Trans. 2012; 41:13105–13111. [PubMed: 23018189]

(42). Ji Z, Natu G, Wu Y. Cyclometalated Ruthenium Sensitizers Bearing a Triphenylamino Group for p-Type NiO Dye-Sensitized Solar Cells. ACS Appl Mater Interfaces. 2013; 5:8641–8648. [PubMed: 23927567]

(43). Ji Z, Wu Y. Photoinduced Electron Transfer Dynamics of Cyclometalated Ruthenium (II)–Naphthalenediimide Dyad at NiO Photocathode. J Phys Chem C. 2013; 117:18315–18324.

(44). Brautigam M, Kubel J, Schulz M, Vos JG, Dietzek B. Hole injection dynamics from two structurally related Ru-bipyridine complexes into NiOx is determined by the substitution pattern of the ligands. Phys Chem Chem Phys. 2015; 17:7823–7830. [PubMed: 25716520]

(45). Andrew N, Michael F, Robert K, Yi-Bing C, Udo B. Dye-sensitized nickel(II) oxide photocathodes for tandem solar cell applications. Nanotechnology. 2008; 19:295304. [PubMed: 21730603]

(46). Sheehan S, Naponiello G, Odobel F, Dowling DP, Di Carlo A, Dini D. Comparison of the photoelectrochemical properties of RDS NiO thin films for p-type DSCs with different organic

and organometallic dye-sensitizers and evidence of a direct correlation between cell efficiency and charge recombination. J Solid State Electrochem. 2015; 19:975–986.

(47). Zhang L, Favereau L, Farre Y, Mijangos E, Pellegrin Y, Blart E, Odobel F, Hammarstrom L. Ultrafast and slow charge recombination dynamics of diketopyrrolopyrrole-NiO dye sensitized solar cells. Phys Chem Chem Phys. 2016; 18:18515–18527. [PubMed: 27338174]

(48). D'Amario L, Antila LJ, Pettersson Rimgard B, Boschloo G, Hammarström L. Kinetic Evidence of Two Pathways for Charge Recombination in NiO-Based Dye-Sensitized Solar Cells. J Phys Chem Lett. 2015; 6:779–783. [PubMed: 26262652]

(49). Gillaizeau-Gauthier I, Odobel F, Alebbi M, Argazzi R, Costa E, Bignozzi CA, Qu P, Meyer GJ. Phosphonate-Based Bipyridine Dyes for Stable Photovoltaic Devices. Inorg Chem. 2001; 40:6073–6079. [PubMed: 11681930]

(50). Amouyal E, Homsi A, Chambron J-C, Sauvage J-P. Synthesis and study of a mixed-ligand ruthenium(II) complex in its ground and excited states: bis(2,2'-bipyridine)(dipyrido[3,2-a:2',3'-c]phenazine-N^4N^5)ruthenium(II). J Chem Soc Dalton Trans. 1990:1841–1845.

(51). Mabrouk PA, Wrighton MS. Resonance Raman spectroscopy of the lowest excited state of derivatives of tris(2,2'-bipyridine)ruthenium(II): substituent effects on electron localization in mixed-ligand complexes. Inorg Chem. 1986; 25:526–531.

(52). Massin J, Braütigam M, Kaeffer N, Queyriaux N, Field MJ, Schacher FH, Popp J, Chavarot-Kerlidou M, Dietzek B, Artero V. Dye-sensitized PS-b-P2VP-templated nickel oxide films for photoelectrochemical applications. Interface Focus. 2015; 5:20140083. [PubMed: 26052420]

(53). Brautigam M, Kubel J, Schulz M, Vos JG, Dietzek B. Hole injection dynamics from two structurally related Ru-bipyridine complexes into NiO(x) is determined by the substitution pattern of the ligands. Phys Chem Chem Phys. 2015; 17:7823–7830. [PubMed: 25716520]

(54). Karnahl M, Kuhnt C, Ma F, Yartsev A, Schmitt M, Dietzek B, Rau S, Popp J. Tuning of photocatalytic hydrogen production and photoinduced intramolecular electron transfer rates by regioselective bridging ligand substitution. ChemPhysChem. 2011; 12:2101–2109. [PubMed: 21681884]

(55). Bräutigam M, Wächtler M, Rau S, Popp J, Dietzek B. Photophysical dynamics of a ruthenium polypyridine dye controlled by solvent pH. J Phys Chem C. 2012; 116:1274–1281.

(56). Wächtler M, Kupfer S, Guthmuller J, Rau S, González L, Dietzek B. Structural control of photoinduced dynamics in 4H-Imidazole-ruthenium dyes. J Phys Chem C. 2012; 116:25664–25676.

(57). Dietzek B, Tschierlei S, Hermann G, Yartsev A, Pascher T, Sundström V, Schmitt M, Popp J. Protochlorophyllide a: A comprehensive photophysical picture. ChemPhysChem. 2009; 10:144–150. [PubMed: 18855967]

(58). Kovalenko SA, Dobryakov AL, Ruthmann J, Ernsting NP. Femtosecond spectroscopy of condensed phases with chirped supercontinuum probing. Phys Rev A. 1999; 59:2369–2384.

(59). Dietzek B, Pascher T, Sundström V, Yartsev A. Appearance of coherent artifact signals in femtosecond transient absorption spectroscopy in dependence on detector design. Laser Physics Letters. 2007; 4:38.

(60). Queffelec C, Petit M, Janvier P, Knight DA, Bujoli B. Surface modification using phosphonic acids and esters. Chem Rev. 2012; 112:3777–3807. [PubMed: 22530923]

(61). Mutin PH, Guerrero G, Vioux A. Hybrid materials from organophosphorus coupling molecules. J Mater Chem. 2005; 15:3761–3768.

(62). Zhang L, Cole JM. Anchoring groups for dye-sensitized solar cells. ACS Appl Mater Interfaces. 2015; 7:3427–3455. [PubMed: 25594514]

(63). Hanson K, Brennaman MK, Luo H, Glasson CRK, Concepcion JJ, Song W, Meyer TJ. Photostability of Phosphonate-Derivatized, Ru^{II} Polypyridyl Complexes on Metal Oxide Surfaces. ACS Appl Mater Interfaces. 2012; 4:1462–1469. [PubMed: 22316053]

(64). Braumuller M, Schulz M, Sorsche D, Pfeffer M, Schaub M, Popp J, Park B-W, Hagfeldt A, Dietzek B, Rau S. Synthesis and characterization of an immobilizable photochemical molecular device for H_2-generation. Dalton Trans. 2015; 44:5577–5586. [PubMed: 25698297]

(65). Sabatani E, Nikol HD, Gray HB, Anson FC. Emission spectroscopy of $Ru(bpy)_2dppz^{2+}$ in nafion. Probing the chemical environment in cast films. J Am Chem Soc. 1996; 118:1158–1163.

(66). Montalti M, Wadhwa S, Kim WY, Kipp RA, Schmehl RH. Luminescent ruthenium(II) bipyridyl–phosphonic acid complexes: pH dependent photophysical behavior and quenching with divalent metal ions. Inorg Chem. 2000; 39:76–84. [PubMed: 11229038]

(67). Fees J, Kaim W, Moscherosch M, Matheis W, Klima J, Krejcik M, Zalis S. Electronic structure of the "molecular light switch" bis(bipyridine)dipyrido[3,2-a:2',3'-c]phenazineruthenium(2+). Cyclic voltammetric, UV/visible and EPR/ENDOR study of multiply reduced complexes and ligands. Inorg Chem. 1993; 32:166–174.

(68). Umberger JQ, LaMer VK. The kinetics of diffusion controlled molecular and ionic reactions in solution as determined by measurements of the quenching of fluorescence. J Am Chem Soc. 1945; 67:1099–1109.

(69). Campagna S, Puntoriero F, Nastasi F, Bergamini G, Balzani V. Photochemistry and photophysics of coordination compounds: ruthenium. Top Curr Chem. 2007; 280:117–214.

(70). Sun Y, Collins SN, Joyce LE, Turro C. Unusual Photophysical Properties of a Ruthenium(II) Complex Related to $[Ru(bpy)_2(dppz)]^{2+}$ Inorg Chem. 2010; 49:4257–4262. [PubMed: 20353166]

(71). Gibson EA, Le Pleux L, Fortage J, Pellegrin Y, Blart E, Odobel F, Hagfeldt A, Boschloo G. Role of the Triiodide/Iodide Redox Couple in Dye Regeneration in p-Type Dye-Sensitized Solar Cells. Langmuir. 2012; 28:6485–6493. [PubMed: 22432412]

(72). Chen W, Rein FN, Rocha RC. Homogeneous photocatalytic oxidation of alcohols by a chromophore–catalyst dyad of ruthenium complexes. Angew Chem Int Ed. 2009; 48:9672–9675.

(73). Pavlishchuk VV, Addison AW. Conversion constants for redox potentials measured versus different reference electrodes in acetonitrile solutions at 25°C. Inorg Chim Acta. 2000; 298:97–102.

(74). Gillaizeau-Gauthier I, Odobel F, Alebbi M, Argazzi R, Costa E, Bignozzi CA, Qu P, Meyer GJ. Phosphonate-based bipyridine dyes for stable photovoltaic devices. Inorg Chem. 2001; 40:6073–6079. [PubMed: 11681930]

(75). Hamd W, Chavarot-Kerlidou M, Fize J, Muller G, Leyris A, Matheron M, Courtin E, Fontecave M, Sanchez C, Artero V, Laberty-Robert C. Dye-sensitized nanostructured crystalline mesoporous tin-doped indium oxide films with tunable thickness for photoelectrochemical applications. J Mater Chem A. 2013; 1:8217–8225.

(76). Macdonald TJ, Mange YJ, Dewi MR, Islam HU, Parkin IP, Skinner WM, Nann T. $CuInS_2$/ZnS nanocrystals as sensitisers for NiO photocathodes. J Mater Chem A. 2015; 3:13324–13331.

(77). Peck MA, Langell MA. Comparison of Nanoscaled and Bulk NiO Structural and Environmental Characteristics by XRD, XAFS, and XPS. Chem Mater. 2012; 24:4483–4490.

(78). Piper DJE, Barbante GJ, Brack N, Pigram PJ, Hogan CF. Highly stable ECL active films formed by the electrografting of a diazotized ruthenium complex generated in situ from the amine. Langmuir. 2011; 27:474–480. [PubMed: 21117679]

(79). Viornery C, Chevolot Y, Léonard D, Aronsson B-O, Péchy P, Mathieu HJ, Descouts P, Grätzel M. Surface modification of titanium with phosphonic acid to improve bone bonding: Characterization by XPS and ToF-SIMS. Langmuir. 2002; 18:2582–2589.

(80). Adden N, Gamble LJ, Castner DG, Hoffmann A, Gross G, Menzel H. Phosphonic acid monolayers for binding of bioactive molecules to titanium surfaces. Langmuir. 2006; 22:8197–8204. [PubMed: 16952262]

(81). Hoertz PG, Chen Z, Kent CA, Meyer TJ. Application of high surface area tin-doped indium oxide nanoparticle films as transparent conducting electrodes. Inorg Chem. 2010; 49:8179–8181. [PubMed: 20712331]

(82). Direct proton reduction was eliminated on the basis of a 12h continuous electrolysis experiment performed in our previous study (see ref. 52) under conditions similar to whose employed here; no hydrogen could be detected in the headspace of the cell.

(83). Khnayzer RS, Thoi VS, Nippe M, King AE, Jurss JW, El Roz KA, Long JR, Chang CJ, Castellano FN. Towards a comprehensive understanding of visible-light photogeneration of hydrogen from water using cobalt(II) polypyridyl catalysts. Energy Environ Sci. 2014; 7:1477–1488.

(84). Bachmann C, Guttentag M, Spingler B, Alberto R. 3d Element complexes of pentadentate bipyridine-pyridine-based ligand scaffolds: structures and photocatalytic activities. Inorg Chem. 2013; 52:6055–6061. [PubMed: 23641941]

(85). Varma S, Castillo CE, Stoll T, Fortage J, Blackman AG, Molton F, Deronzier A, Collomb M-N. Efficient photocatalytic hydrogen production in water using a cobalt(III) tetraaza-macrocyclic catalyst: electrochemical generation of the low-valent Co(I) species and its reactivity toward proton reduction. Phys Chem Chem Phys. 2013; 15:17544–17552. [PubMed: 24030544]

(86). Deponti E, Luisa A, Natali M, Iengo E, Scandola F. Photoinduced hydrogen evolution by a pentapyridine cobalt complex: elucidating some mechanistic aspects. Dalton Trans. 2014; 43:16345–16353. [PubMed: 25237910]

(87). Wallin S, Davidsson J, Modin J, Hammarström L. Femtosecond transient Absorption anisotropy study on $[Ru(bpy)_3]^{2+}$ and $[Ru(bpy)(py)_4]^{2+}$. Ultrafast interligand randomization of the MLCT State. J Phys Chem A. 2005; 109:4697–4704. [PubMed: 16833810]

(88). Kuhnt C, Karnahl M, Tschierlei S, Griebenow K, Schmitt M, Schafer B, Krieck S, Gorls H, Rau S, Dietzek B, Popp J. Substitution-controlled ultrafast excited-state processes in Ru-dppz-derivatives. Phys Chem Chem Phys. 2010; 12:1357–1368. [PubMed: 20119614]

(89). Kalyanasundaram K, Zakeeruddin SM, Nazeeruddin MK. Ligand to metal charge transfer transitions in Ru(III) and Os(III) complexes of substituted 2,2'-bipyridines. Coord Chem Rev. 1994; 132:259–264.

(90). Coates CG, Callaghan P, McGarvey JJ, Kelly JM, Jacquet L, Kirsch-De Mesmaeker A. Spectroscopic studies of structurally similar DNA-binding Ruthenium (II) complexes containing the dipyridophenazine ligand. J Mol Struct. 2001; 598:15–25.

(91). McCusker CE, McCusker JK. Synthesis and spectroscopic characterization of CN-substituted bipyridyl complexes of Ru(II). Inorg Chem. 2011; 50:1656–1669. [PubMed: 21288049]

(92). Farnum BH, Ward WM, Meyer GJ. Flash-quench studies on the one-electron reduction of triiodide. Inorg Chem. 2013; 52:840–847. [PubMed: 23276296]

(93). Boschloo G, Hagfeldt A. spectroelectrochemistry of nanostructured NiO. J Phys Chem B. 2001; 105:3039–3044.

(94). Morandeira A, Boschloo G, Hagfeldt A, Hammarström L. Coumarin 343−NiO films as nanostructured photocathodes in dye-sensitized solar cells: ultrafast electron transfer, effect of the I_3^-/I^- redox couple and mechanism of photocurrent generation. J Phys Chem C. 2008; 112:9530–9537.

(95). Morandeira A, Fortage J, Edvinsson T, Le Pleux L, Blart E, Boschloo G, Hagfeldt A, Hammarström L, Odobel F. Improved photon-to-current conversion efficiency with a nanoporous p-type NiO electrode by the use of a sensitizer-acceptor dyad. J Phys Chem C. 2008; 112:1721–1728.

(96). Gibson EA, Smeigh AL, Le Pleux L, Fortage J, Boschloo G, Blart E, Pellegrin Y, Odobel F, Hagfeldt A, Hammarström L. A p-type NiO-based dye-sensitized solar cell with an open-circuit voltage of 0.35 V. Angew Chem Int Ed. 2009; 48:4402–4405.

(97). Dietzek B, Kiefer W, Blumhoff J, Böttcher L, Rau S, Walther D, Uhlemann U, Schmitt M, Popp J. Ultrafast excited-state excitation dynamics in a quasi-two-dimensional light-harvesting antenna based on ruthenium(II) and palladium(II) chromophores. Chem Eur J. 2006; 12:5105–5115. [PubMed: 16628758]

(98). Henry W, Coates CG, Brady C, Ronayne KL, Matousek P, Towrie M, Botchway SW, Parker AW, Vos JG, Browne WR, McGarvey JJ. The early picosecond photophysics of Ru(II) polypyridyl complexes: a tale of two timescales. J Phys Chem A. 2008; 112:4537–4544. [PubMed: 18438991]

(99). Schwalbe M, Karnahl M, Tschierlei S, Uhlemann U, Schmitt M, Dietzek B, Popp J, Groake R, Vos JG, Rau S. The switch that wouldn't switch - unexpected luminescence from a ruthenium(ii)-dppz-complex in water. Dalton Trans. 2010; 39:2768–2771. [PubMed: 20200701]

(100). Marrani AG, Novelli V, Sheehan S, Dowling DP, Dini D. Probing the redox states at the surface of electroactive nanoporous NiO thin films. ACS Appl Mater Interfaces. 2014; 6:143–152. [PubMed: 24325361]

(101). Batista ER, Martin RL. On the excited states involved in the luminescent probe $[Ru(bpy)_2dppz]^{2+}$ J Phys Chem A. 2005; 109:3128–3133. [PubMed: 16833639]

(102). Lundin NJ, Walsh PJ, Howell SL, Blackman AG, Gordon KC. A synthetic, structural, spectroscopic and DFT study of Re^{I}, Cu^{I}, Ru^{II} and Ir^{III} complexes containing functionalised dipyrido[3,2-a:2′,3′-c]phenazine (dppz). Chem Eur J. 2008; 14:11573–11583. [PubMed: 19021163]

Europe PMC Funders Author Manuscripts

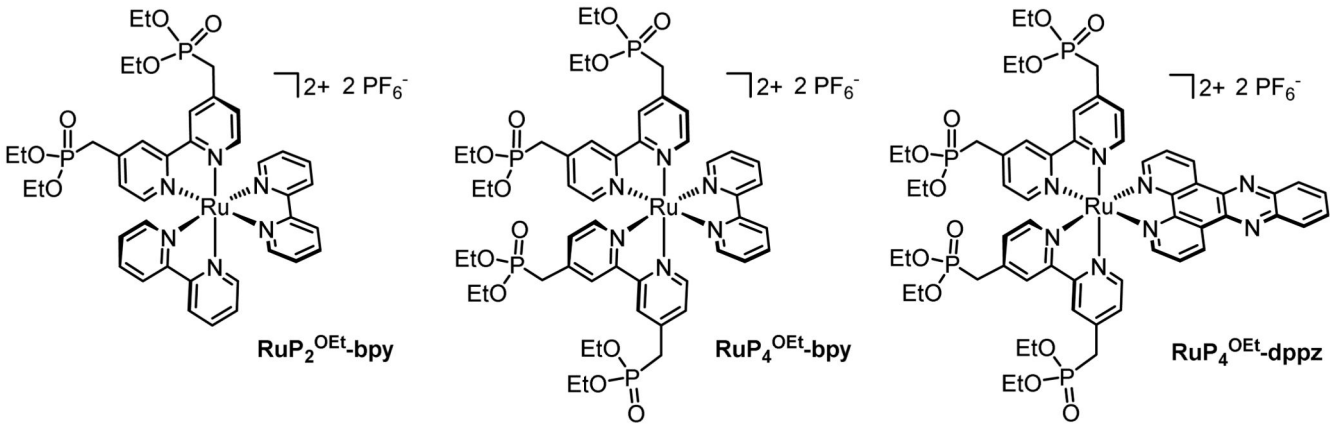

Figure 1.

Structures of the ruthenium polypyridyl complexes $[Ru^{II}(4,4'\text{-}(CH_2PO_3Et_2)_2\text{-bpy})(bpy)_2](PF_6)_2$ (**RuP_2^{OEt}-bpy**), $[Ru^{II}(4,4'\text{-}(CH_2PO_3Et_2)_2\text{-bpy})_2(bpy)](PF_6)_2$ (**RuP_4^{OEt}-bpy**) and $[Ru^{II}(4,4'\text{-}(CH_2PO_3Et_2)_2\text{-bpy})_2(dppz)](PF_6)_2$ (**RuP_4^{OEt}-dppz**) employed in this study.

Europe PMC Funders Author Manuscripts

Europe PMC Funders Author Manuscripts

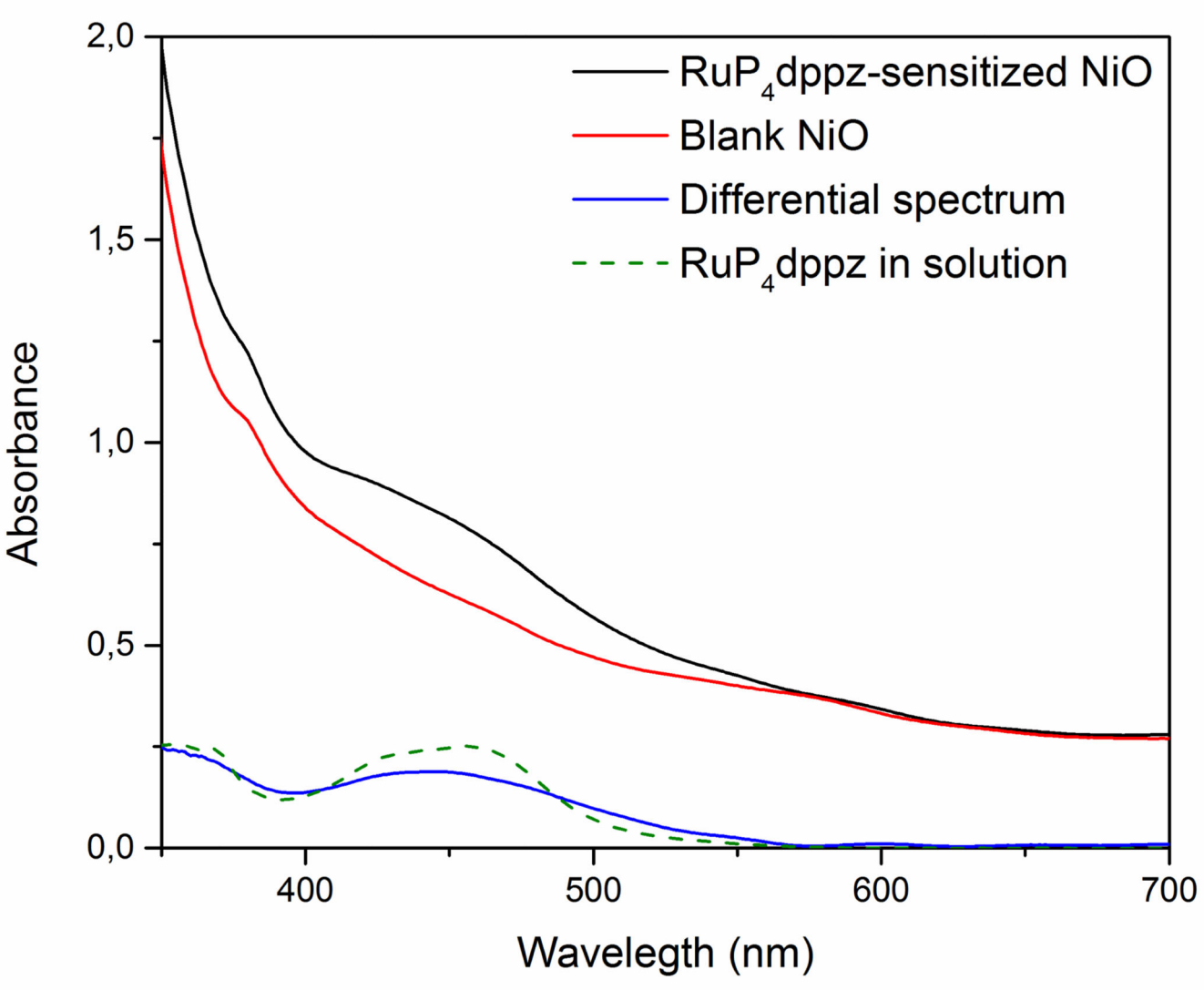

Figure 2.

Absorption spectra of blank NiO (red line), the same film sensitized with **RuP_4^{OH}-dppz** (**NiO|RuP_4-dppz**, black line) and the corresponding differential spectrum (blue line).

Europe PMC Funders Author Manuscripts

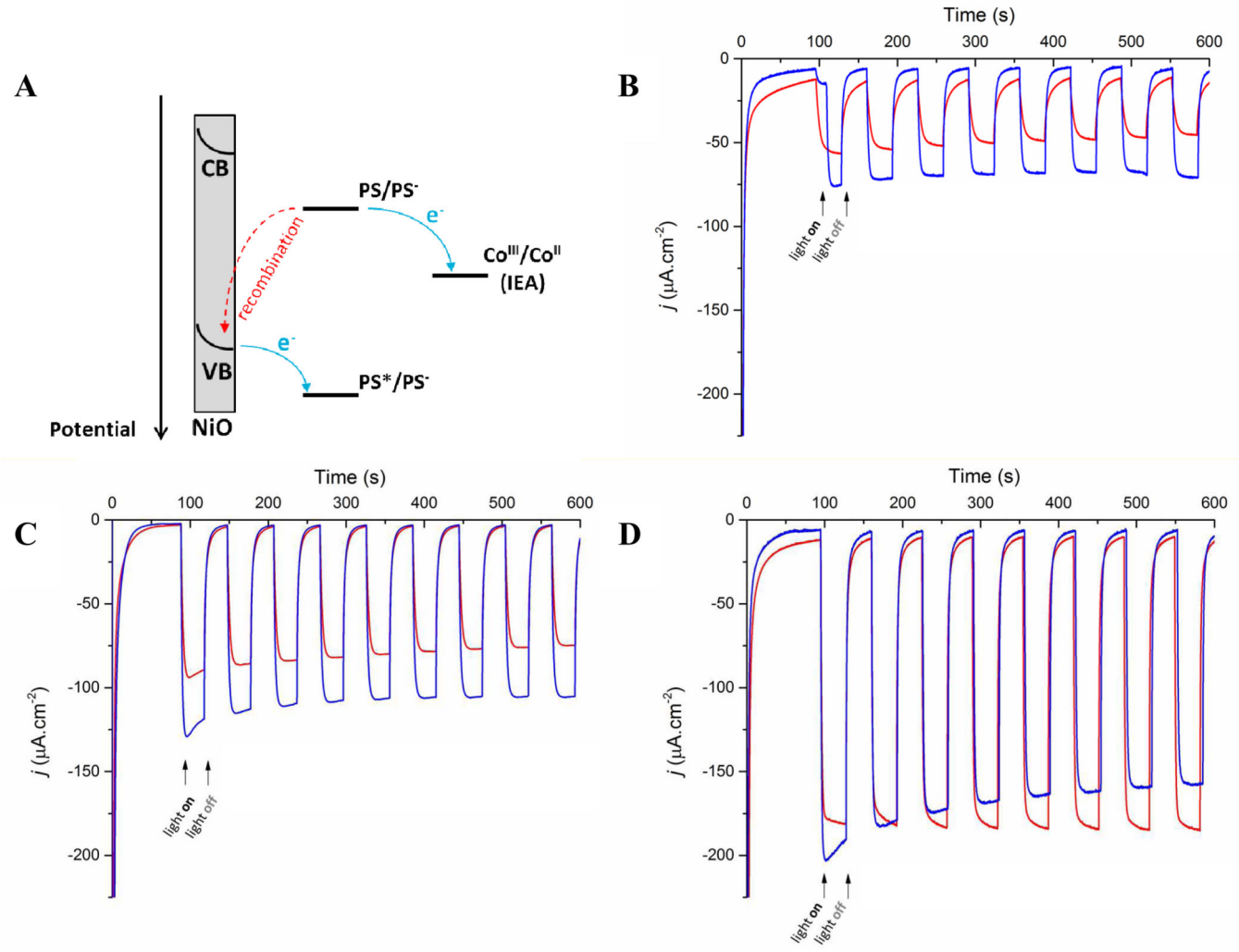

Figure 3.

Schematic principle for the electron transfer processes taking place after irradiation of the dye-sensitized electrode in the presence of irreversible electron acceptor (IEA) (**A**); cathodic photocurrent densities recorded on **NiO|RuP$_2$-bpy** (**B**), **NiO|RuP$_4$-bpy** (**C**) and **NiO|RuP$_4$-dppz** (**D**) electrodes, in the presence of $[Co(NH_3)_5Cl]Cl_2$ (20 mM) as IEA. The measurements were carried out under chopped light irradiation, either in acetate buffer 0.1 M pH 4.5 (red) or phosphate buffer 0.1 M pH 7.0 (blue) at an applied potential of 0 V *vs* Ag/AgCl.

Europe PMC Funders Author Manuscripts

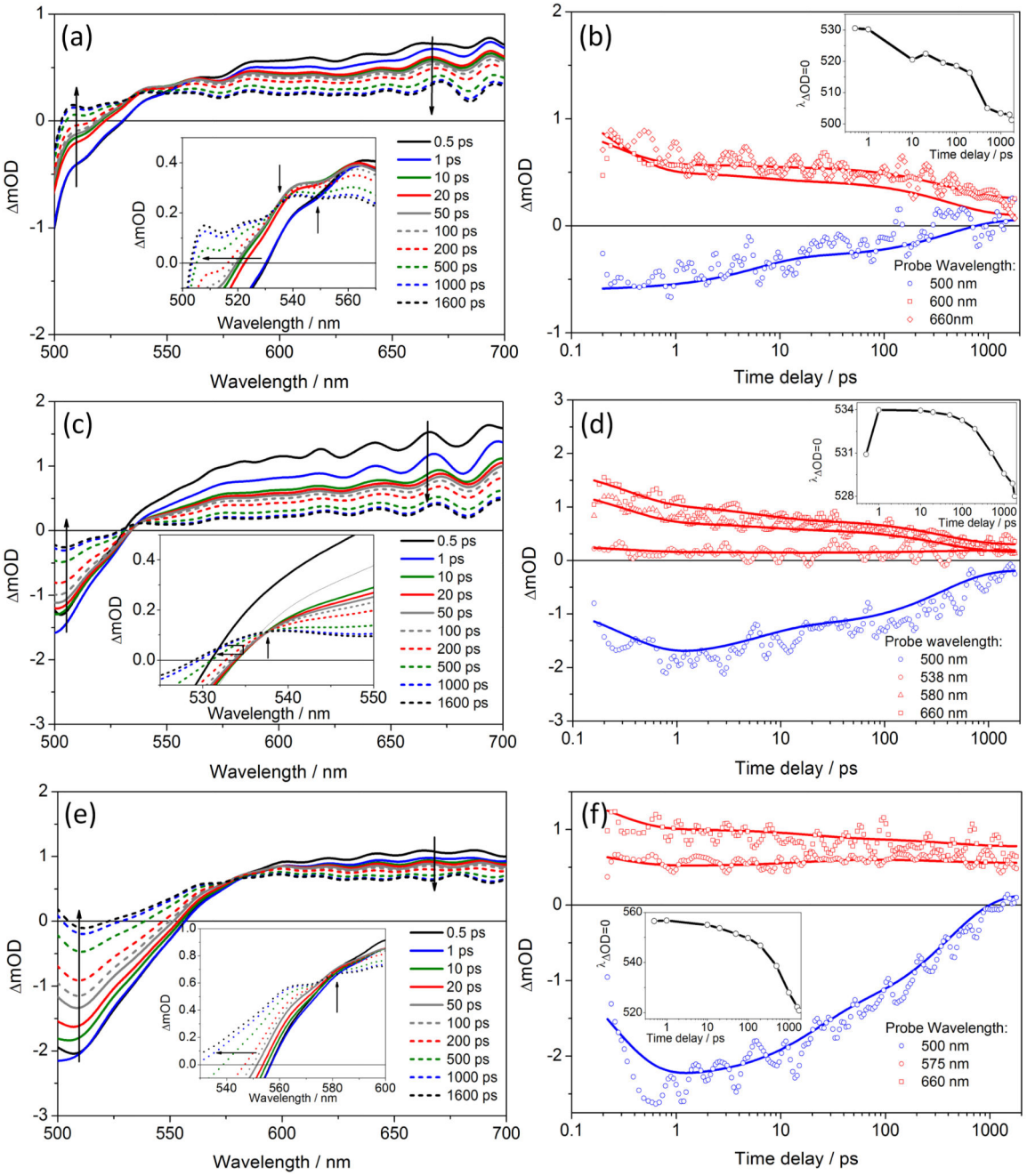

Figure 4.

(left) Transient absorption difference spectra upon excitation at 480 nm at different delay times and (right) kinetic traces at different probe wavelength of (a,b) **NiO|RuP$_4$-bpy**, (c,d) **NiO|RuP$_4$-bpy** and (e,f) **NiO|RuP$_4$-dppz**. Insets of left figure show evolution of absorption difference spectra at around ΔOD=0 and at isobestic point, while insets of right figure show dynamic shift of the probe wavelength at which ΔOD=0 is observed.

Europe PMC Funders Author Manuscripts

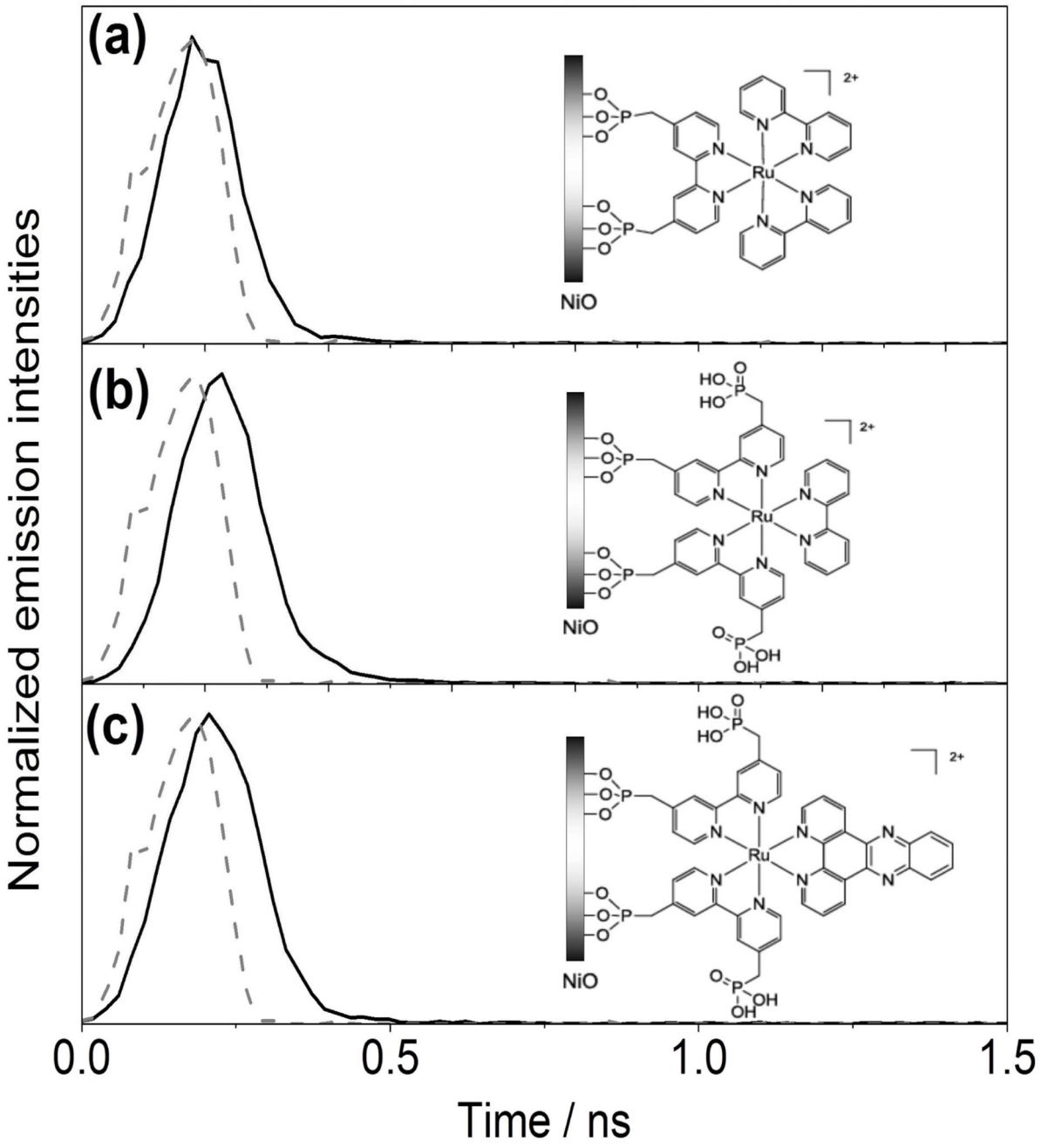

Figure 5.

Time-resolved luminescence spectra of (a) **NiO|RuP$_2$-bpy**, (b) **NiO|RuP$_4$-bpy**, and (c) **NiO|RuP$_4$-dppz**. Instrumental responses of time-resolved luminescence measurement are indicated by dashed grey lines.

Europe PMC Funders Author Manuscripts

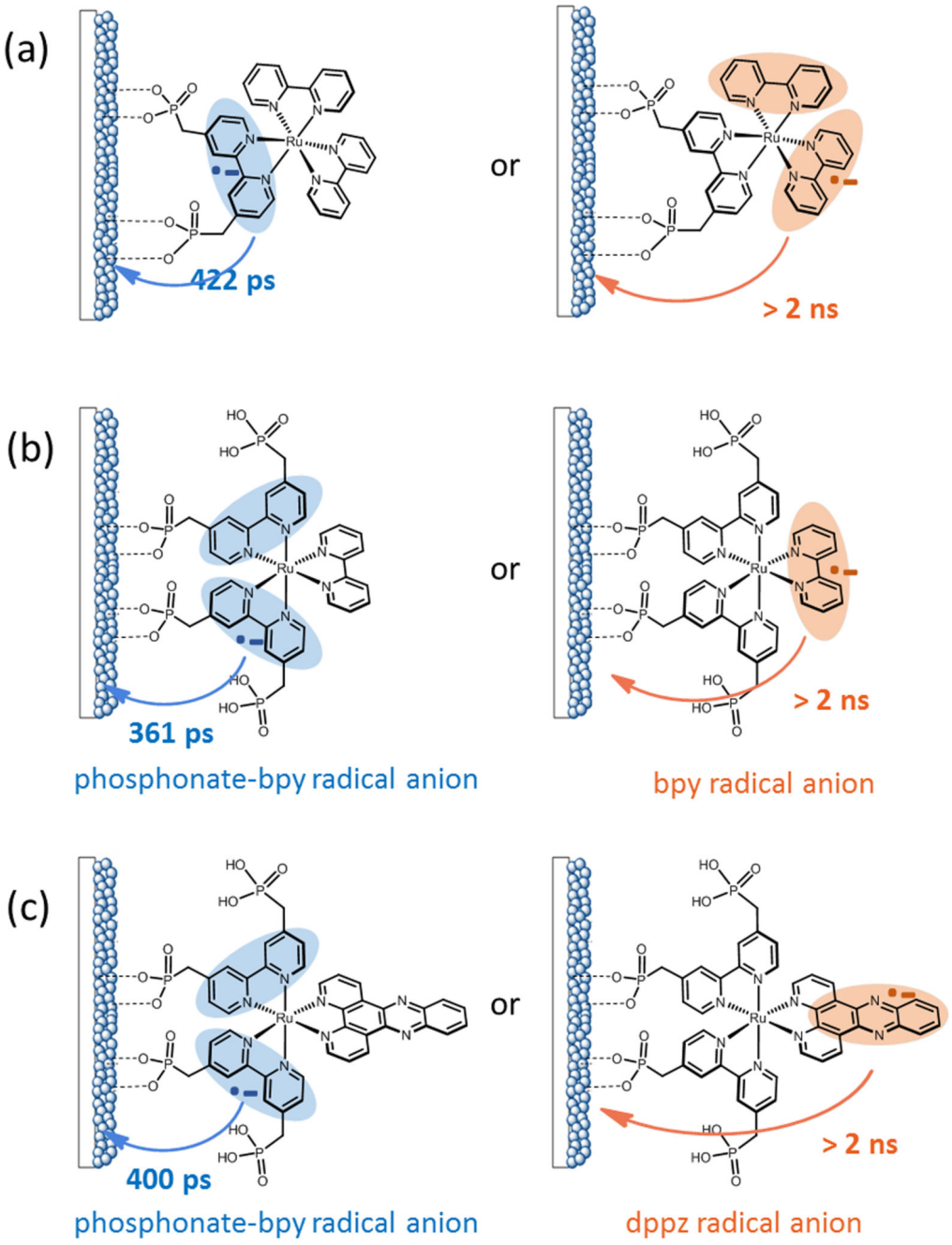

Figure 6.

Photophysical scheme of different recombination pathways on (a) **NiO|RuP$_2$-bpy**, (b) **NiO|RuP$_4$-bpy** and (c) **NiO|RuP$_4$-dppz**.

Europe PMC Funders Author Manuscripts

Table 1

Photophysical[a] and redox properties[b] of complexes **RuP_2^{OEt}-bpy**, **RuP_4^{OEt}-bpy** and **RuP_4^{OEt}-dppz** together with $[Ru(bpy)_3](PF_6)_2$ and $[Ru(bpy)_2(dppz)](PF_6)_2$ as reference complexes.

Dye	λ_{abs} (ε)[c]	λ_{em}(Φ_{PL})[d]	τ[e]	$E_{0\text{-}0}$[f]	E_{ox}	E_{red1}	E_{red2}	E_{red3}	E_{red4}	ΔG_{inj}[g]	ΔG_{reg}[h]
RuP_2^{OEt}-bpy	288 (85368), 453 (14918)	625 (2.9)	174	2.12	+0.87	—	–1.73	–1.93	–2.16	–0.51	–1.05
RuP_4^{OEt}-bpy	289 (91810), 457 (14665)	625 (2.0)	197	2.12	+0.87	—	–1.70	–1.89	–2.15	–0.54	–1.02
RuP_4^{OEt}-dppz	283 (97800), 358 (16590), 457 (16455)	646 (4.1)	192	2.13	+0.89	–1.35	–1.72	–1.92	–2.33	–0.53	–0.67
$[Ru(bpy)_3](PF_6)_2$	286 (85030), 451 (14500)	627	-	2.12	+0.89	—	–1.73	–1.92	–2.17	—	—
$[Ru(bpy)_2(dppz)](PF_6)_2$	283 (98036), 358 (17894), 450 (16681)	633	-	2.13	+0.91	-1.35	–1.79	–2.01	–2.31	—	—

[a] Absorption and emission spectra were recorded in acetonitrile.

[b] in V *vs* Fc^+/Fc. Cyclic voltammograms were recorded at a complex concentration of 1 mM in a 0.1 M solution of *n*-Bu_4NBF_4 in degassed acetonitrile and at a scan rate of 100 $mV.s^{-1}$.

[c] λ_{abs} in nm; ε in $L.mol^{-1}.cm^{-1}$.

[d] λ_{em} in nm; Φ_{PL} in %. Quantum yields were determined using Fluorescein (0.1M NaOH, Φ_{PL}= 95%) as reference.68

[e] τ in ns. Emission lifetimes were measured in air-equilibrated acetonitrile.

[f] in eV. The 0–0 transition energy ($E_{0\text{-}0}$) was considered similar to the respective parent complex, $[Ru(bpy)_3]^{2+}$ 69 and $[Ru(bpy)_2(dppz)]^{2+}$ respectively, assuming that the phosphonate anchoring groups do not significantly alter the chromophore properties. For $[Ru(bpy)_2(dppz)]^{2+}$, $E_{0\text{-}0}$ was estimated from the reported maximum emission intensity at 77K,70 with the equation $E_{0\text{-}0}$ = 1240/λ.

[g] in eV. The Gibbs free energy for the hole injection reaction was calculated according to ΔG_{inj} = e[E_{VB}(NiO) – E(PS*/PS^-)]; with E_{VB}(NiO) = –0.12V vs $Fc^{+/0}$ 71 and E(PS*/PS^-) = E(PS/PS^-) + $E_{0\text{-}0}$.

[h] in eV. The Gibbs free energy for the dye regeneration by electron transfer to the irreversible electron acceptor $[Co^{III}(NH_3)_5Cl]Cl_2$ was calculated according to ΔG_{reg} = e[E(PS/PS^-) – E(Co^{III}/Co^{II})]; the reduction potential E(Co^{III}/Co^{II}) (–0.30 V vs SCE)72 was converted to $Fc^{+/0}$ by subtracting 0.38 V.73

Europe PMC Funders Author Manuscripts

Table 2

Sensitizer	Cathodic photocurrent density (*j*)[a]		Cathodic photocurrent density per nmol of grafted photosensitizer[d]		Stability (over 10 min)	
	pH 4.5[b]	pH 7[c]	pH 4.5[b]	pH 7[c]	pH 4.5[b]	pH 7[c]
RuP_2-bpy	−50	−70	5.6	7.9	80 %	90 %
RuP_4-bpy	−87	−120	7.9	10.9	82 %	85 %
RuP_4-dppz	−170	−190	12.1	13.6	100 %	80 %

[a] in $\mu A.cm^{-2}$, measured on the first irradiation cycle, dark current subtracted; 0.50 cm^2 electrode surface.

[b] sodium acetate buffer, 0.1 M.

[c] potassium phosphate buffer, 0.1 M.

[d] j/Γ in $\mu A.nmol^{-1}.cm^{-2}$.

Europe PMC Funders Author Manuscripts

Table 3

The fitted time constants (τ) and relative amplitude decay measured at integrated spectral range 650 - 700 nm (A) from transient absorption data. The weights of the individual components are derived following a protocol by Wu and coworkers.40,43

	NiO|RuP$_2$-bpy	**NiO|RuP$_4$-bpy**	**NiO|RuP$_4$-dppz**
τ_1 / ps (A)	0.3 (0.25)	0.3 (0.24)	0.2 (0.19)
τ_2 / ps (A)	5.8 (0.13)	6.1 (0.17)	19.5 (0.07)
τ_3 / ps (A)	422 (0.25)	361 (0.30)	400 (0.17)
τ_4 / ns (A)	> 2 (0.37)	> 2 (0.29)	> 2 (0.57)